Chemical looping for biomass gasification
development of a phenomenological model

Timmers, M.W.

Award date:
2015

Technische Universiteit
Eindhoven
University of Technology

Process Engineering Multiphase Reactor group (SMR)
Department of Chemical Engineering and Chemistry

Kranenveld 14, 5612 AZ Eindhoven
P.O. Box 513, 5600 MB Eindhoven
The Netherlands
www.tue.nl

Author: M.W. Timmers

ID nr. 0743140

Graduation committee:
Prof. Dr. Ir. M. van Sint Annaland
Dr. F. Gallucci
Dr. Q. Wang
I. Campos Velarde, MSc

12-05-2015

Chemical looping for biomass gasification

Development of a phenomenological model

Where innovation starts

Abstract

Fossil fuel sources are limited and the energy consumption in the world is increasing, resulting into a need for new and sustainable energy sources. The production of energy and chemicals from fossil fuels causes the formation of carbon dioxide. CO_2 affects the climate on earth, and its concentration in the atmosphere is increasing. Biomass is a promising energy source as it is CO_2 neutral and it is infinitely available. Biomass can be gasified to produce energy containing compounds as syngas. Gasification of biomass is mostly done in a fluidized bed. Recently, biomass has been researched for use in a dual fluidized bed configuration with a circulation solid [1]. Biomass is gasified in the gasification zone and the produced tar and char are burned in the combustor. The heat produced in the combustor is delivered to the gasifier by solid bed material. Catalytic materials can be used as active bed material. They can catalyze char gasification and tar destruction.

Experimental work has been done on the reduction of tars in biomass gasification, but only limited theoretical work has been drawn up. In this graduation project, a phenomenological model for indirect biomass gasification using an oxygen carrier as bed material for the optimal production of syngas was developed. Olivine and ilmenite were used as oxygen carriers.

Removal of tars is a vital technological barrier hindering the development of biomass gasification. The activity of olivine and ilmenite towards tar steam reforming was compared experimentally. They were tested in a packed bed reactor with toluene as a model tar component. Olivine proved to be more suitable as a catalytic bed material due to the lack of side products produced in the toluene steam reforming reaction. Different samples of olivine and ilmenite were analyzed by SEM and EDX; pure, after activation and after reaction. SEM and EDX pointed out that great structural changes occur in both minerals due to activation and reaction, which is caused by migration of several elements through the material.

A TNEE model with sand as a solid bed material in Aspen Plus was already in place from a prior graduation project [2]. This model was first improved and simplified. Tars were lumped into only toluene as a model tar component. Hereafter, this model was expanded to include the catalytic activity of a tar reducing active bed material. As only kinetics for olivine doped with nickel could be found [3], these were included in the model. The activity of the Ni-olivine catalyst was theoretically compared to the activity of olivine from experiments. Olivine was found to be less active. As a final step, iron hydroxide reduction and oxidation reactions were added to the model to simulate the oxygen carrier capabilities of the active bed material.

Further research is necessary to determine if the structural changes in olivine and ilmenite are permanent and if they improve their oxygen carrier or catalytic abilities. This could be done by doing consecutive oxidation and reduction cycles with TGA. To model the gas-solid reactions better, MATLAB can be used for representation of the dense zone in the gasifier or for the complete gasifier. More detailed modeling of the gas-solid reactions will help gain more insight in the reactions that occur.

Contents

Abstract 1

Contents 2

1. Introduction 4

1.1. Energy outlook 4

1.2. Biomass as a renewable energy source 4

2. Theoretical background of biomass gasification 5

2.1. Biomass gasification 5

2.2. Chemical looping 6

2.3. Chemical looping for biomass gasification 6

2.3.1. Gasifier 8

2.3.2. Combustor 8

2.4. The MILENA reactor 9

2.5. The TNEE reactor 9

2.6. Tars produced in biomass gasification 9

3. Oxygen carriers as bed material 10

4. Project outline 12

5. Oxygen carriers 13

5.1. Structures and composition 13

5.2. Properties 14

5.3. Use in chemical looping 14

5.4. Catalytic tar decomposition 16

5.5. Reactions catalyzed by oxygen carriers 17

6. Experimental analysis of oxygen carrier activity 18

6.1. Experimental setup 18

6.2. Blank experiments 19

6.2.1. Toluene steam reforming 19

6.2.2. Gas reactions 21

6.3. Toluene steam reforming reaction experiments with olivine and ilmenite 23

6.4. Gas reaction experiments with olivine and ilmenite 27

6.5. Carbon burning experiments 30

6.6. SEM and EDX analysis 31

6.7. Conclusion of the experimental analysis of oxygen carriers 38

7. Phenomenological model 40
7.1. TNEE model with sand as bed material 40
7.2. Expansion and improvement of the TNEE model with sand 42
7.3. Addition of catalytic bed material 43
7.4. Addition of oxidation and reduction reaction 45
8. Conclusions and recommendations 48
9. Acknowledgement 51
10. Works cited 52
11. Appendix 57
11.1. Analysis techniques 57
11.1.1. Thermogravimetric analysis (TGA) 57
11.1.2. Gas chromatography (GC) 57
11.1.3. Gas chromatography – mass spectrometry (GC-MS) 57
11.1.4. Scanning electron microscope (SEM) 57
11.1.5. Energy-dispersive X-ray spectroscopy (EDX) 58
11.2. Wet particle size distribution 58
11.2.1. Experimental set-up 58
11.2.2. Results 58
11.3. Calibration curves of the mass flow controllers of the kinetics set-up 59
11.4. Preliminary toluene steam reforming experiment with olivine 62
11.5. GC calculations and spectra 63
11.5.1. Toluene calibration line 63
11.5.2. Olivine samples 64
11.5.3. Ilmenite samples 66
11.6. GC-MS spectrum 68
11.7. EDX spectrum 69
11.8. Comparison between Ni-olivine kinetics and experimental data for olivine 70

1. Introduction

1.1. Energy outlook

According to the International Energy Outlook of 2013, energy consumption will increase with 56 percent over the next 30 years [4]. As 80 percent of all power production is still based on fossil fuels, (oil, coal and natural gas), sources that are limited, the world faces a serious energy problem. To supply enough energy to fulfill the increasing demand in the future, sustainable energy sources have to be used. In addition to that, the production of energy and chemicals from fossil fuels results in the formation of large amounts of carbon dioxide. CO_2 is the primary greenhouse gas emitted by human activities, which affects the climate on earth, and its concentration in the atmosphere has been increasing steadily since the industrial revolution. In 1997, industrialized countries set up the Kyoto protocol, which contains binding obligations to reduce CO_2 emissions for electricity, coal, and steel plants below their baselines [5]. To reach the goals set by this protocol, emissions have to be cut back; this can be done with alternative forms of fuel production.

1.2. Biomass as a renewable energy source

Biomass has been used as an energy source since man discovered fire. Biomass is a low density energy source, which cannot compete with fossil fuels in modern power production systems. However, converting biomass into gases with gasification, a high-temperature process, seems promising [6]. The product gases produced by this process are carbon monoxide, hydrogen, methane and carbon dioxide. Syngas, the mix of carbon monoxide and hydrogen, can be used in the Fischer-Tropsch synthesis of liquid hydrocarbons [7]. Biomass can be considered as a CO_2 neutral energy source, because the emission of CO_2 caused by the biomass gasification was taken from the atmosphere by photosynthesis during its lifetime. Setbacks linked to biomass as an energy source are the production of tar and char during the processing and the possible competition with food production and nature conservation. If these disadvantages can be sidestepped, biomass as a renewable energy source can be successful.

2. Theoretical background of biomass gasification

Gasification is a partial oxidation process in which a carbon source, such as coal or biomass is broken down into various product gases. Biomass is a renewable fuel that is already widely available throughout the world. Its production and use bring additional environmental and social benefits.

2.1. Biomass gasification

Different technologies are available for biomass gasification; a bubbling fluidized bed, a circulating fluidized bed or indirect gasification. In a BFB, shown on the left of figure 1 the biomass is fed into the fluidized bed, which is fluidized by air or an oxygen-steam mixture [8]. Part of the biomass is combusted to provide the necessary heat for the gasification. The major disadvantage of this technology is the cost due to the use of pure oxygen. Alternatively, a circulating fluidized bed (CFB) can be used, shown in the middle of figure 1. In this type of bed, the entrained bed material is separated from the gas together with remaining char and recycled to the bottom of the reactor. It is a clean process with the ability to absorb pollutants from the producer gas, resulting in a lower emission [8].

In an indirect gasifier, shown in figure 1 on the right, the devolatilisation of the biomass and the combustion of the remaining char are separated. In the first reactor the biomass is gasified. The produced char and the bed material are transported to a second reactor, which is the combustor, where, the char is burned. The bed material is then transported back to the gasifier. The required heat for the gasification is supplied by the bed material which is heated in the combustor. By separating these two steps the product gas is undiluted and air instead of expensive pure oxygen can be used. This increases the heating value of the producer gas [8].

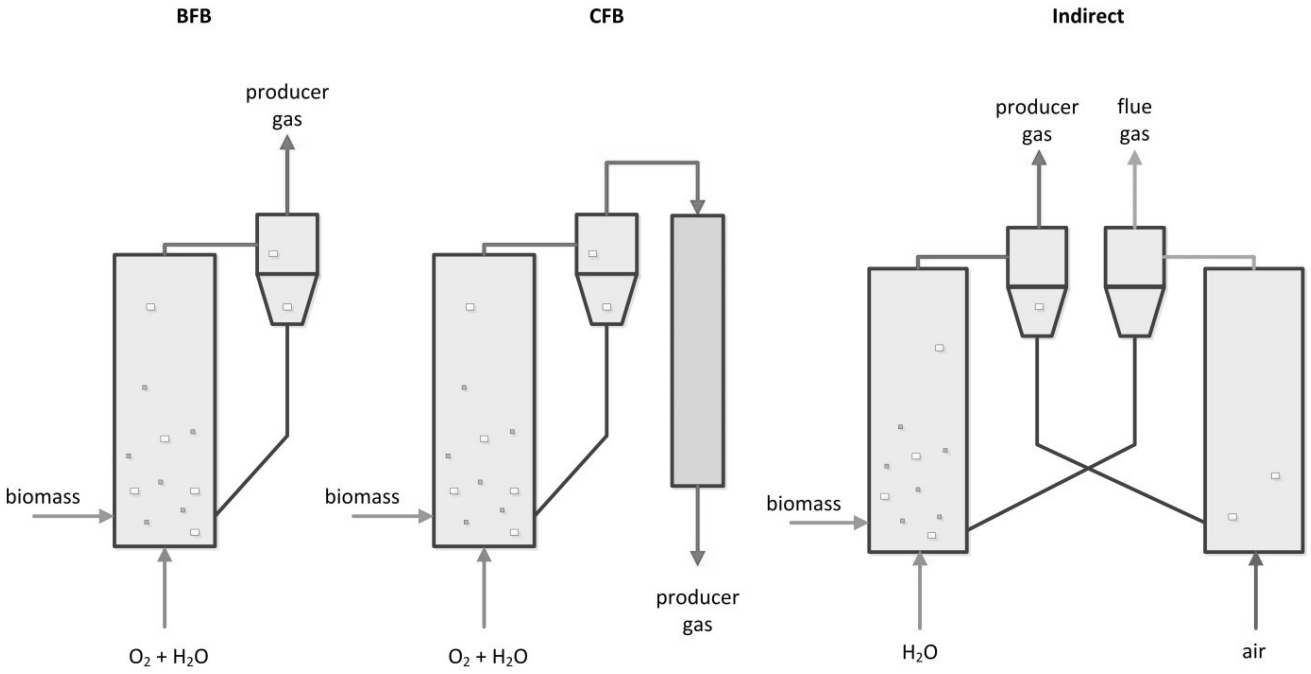

Fig. 1. Schematic form of a BFB, a CFB and an indirect fluidized bed [6].

Indirect gasification leads to lower operational temperatures, better efficiencies and higher conversions. A major downside of biomass gasification is the tar production. Tar is a mixture of high weight hydrocarbons that can foul and block the reactor. More information about tar is given in section 2.6.

2.2. Chemical looping

The indirect biomass gasification can be considered a sort of chemical looping process. Chemical looping is a dual fluidized bed system in which two or more reactions are performed to oxidize a fuel source. A schematic representation of chemical looping combustion can be seen in figure 2. An oxygen carrying compound, also known as an oxygen carrier, is first oxidized in air forming a metal oxide, and then the oxide is reduced using a hydrocarbon as a reducing agent in a second reaction. Energy for the endothermic reforming reactions is provided by indirect combustion that takes place in a separate reactor. The heat produced in the oxidizer is transported to the reducer with the help of the active bed material. The heat exchange can lead to autothermal operation of the two reactors which means that the energy produced by the exothermic reaction is enough to provide the energy needed for the endothermic reaction. Much less extra energy will have to be added to the overall process.

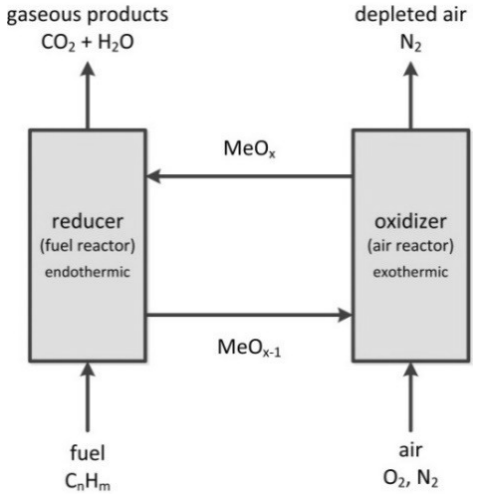

Fig. 2. Chemical looping combustion, the abbreviation MeO_{x-1} is used to describe the oxygen carrier in its reduced form while MeO_x is used for its oxidized form [9].

When using biomass, the fuel source is already CO_2 neutral. It can be combined with CO_2 capture, which can make the overall process CO_2 negative. [9] Carbon Capture and Storage (CCS) can play an important role in the future to diminish CO_2 output to the atmosphere. CCS is the process of capturing waste CO_2 at large point sources such as fossil fuel power plants and transporting it to storages sites underground [10]. Chemical looping is one of the most promising techniques for CO_2 capture. With the two reactors employed in indirect chemical looping, the CO_2 that is produced is not diluted by air needed for combustion and can be easily sequestrated.

2.3. Chemical looping for biomass gasification

Gases can be produced by using biomass gasification as an energy source. The biomass is partly oxidized by a gasification agent (usually steam), which leads to the production of carbon monoxide, hydrogen, methane, carbon dioxide, char and tar. For biomass gasification, chemical looping gasification in two indirectly linked, bubbling fluidized beds is used. One of the BFB is the gasifier which is an endothermic reducer. In the gasifier, the biomass is pyrolyzed. The second BFB is the combustor, which is an exothermic oxidizer. In the combustor, the tar and char that are produced are burned. The gasifier and the combustor are discussed in more detail in the next section. Bed material circulates between the two bubbling fluidized beds and provides heat exchange between them.

A simplified schematic overview of a bubbling fluidized bed with a cyclone can be seen in figure 3. Gas flows into the distributor and is injected through the solid bed which creates a state of fluidization. Bubbles form at the bottom of the reactor and grow (coalesce) along the reactor height. Above the fluidization zone is the freeboard with some entrained particles. Those particles fall back into the fluidization zone, or they are carried away with ascending gas via the outlet.

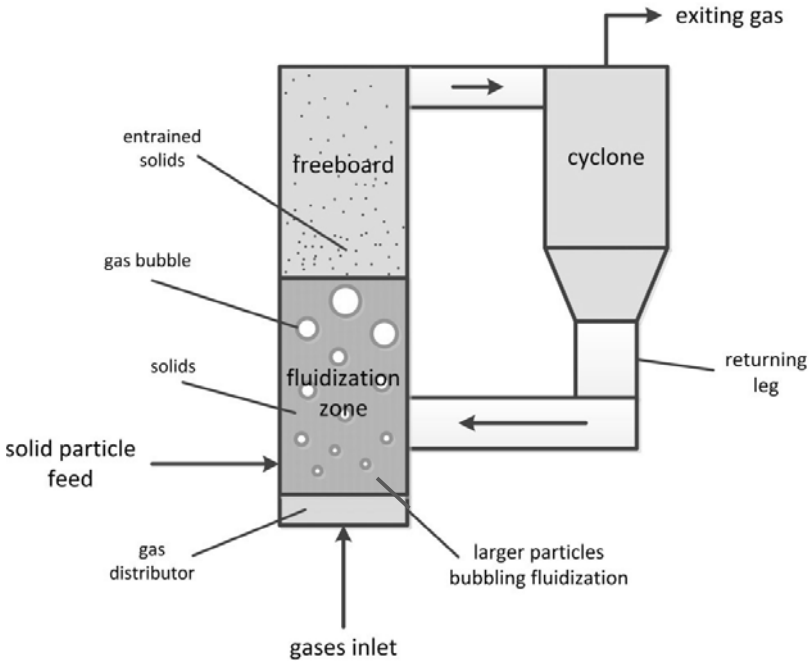

Fig. 3. Schematic display of a bubbling fluidized bed [11].

BFB are fluidized beds in which the bed of solid particles are suspended due to an introduction of fluid that flows through the bed at low velocity. This makes the solid bed material exhibit characteristics of a fluid, which is called fluidization [11]. When the fluid velocity is just above the minimum fluidization velocity the bed particles are relatively stationary and the bed can be treated as if it only consists of two phases, the bubble phase and the emulsion phase.

The rigorous mixing in a fluidized bed enhances its properties by resulting in a uniform temperature, even for highly exothermic or highly endothermic reactions. It improves mass and heat transfer properties as well. A downside to the BFB is that because it is essentially a stirred tank reactor, the solid residence time distribution can be quite wide.

2.3.1. Gasifier

The gasifier is the first bubbling fluidized bed of the chemically looped system. The complete biomass gasification process is schematically represented in figure 4. In the pyrolysis part of this reactor the biomass is instantaneously pyrolyzed using heat from the bed material. The pyrolysis is an irreversible thermochemical decomposition of organic material at elevated temperature in the absence of oxygen. This endothermic reaction leads to the production of several fuel gases, together with different hydrocarbons, divided in gaseous char and tar [12]. This reactor is referred to as the fuel reactor. After devolatilisation of the biomass, many different solid-gas and gas-gas reforming reactions occur in the secondary reaction zone, also known as the freeboard, leading to product gases (CO, H_2, CH_4, CO_2 etc.), tar and char. Tar easily condenses and fouls the downstream equipment which makes it an unwanted substance. Hence the product gases will be separated from the tar in the gas clean-up, after which the tar is transported to the combustor, together with the char and the bed material from the first bubbling fluidized bed.

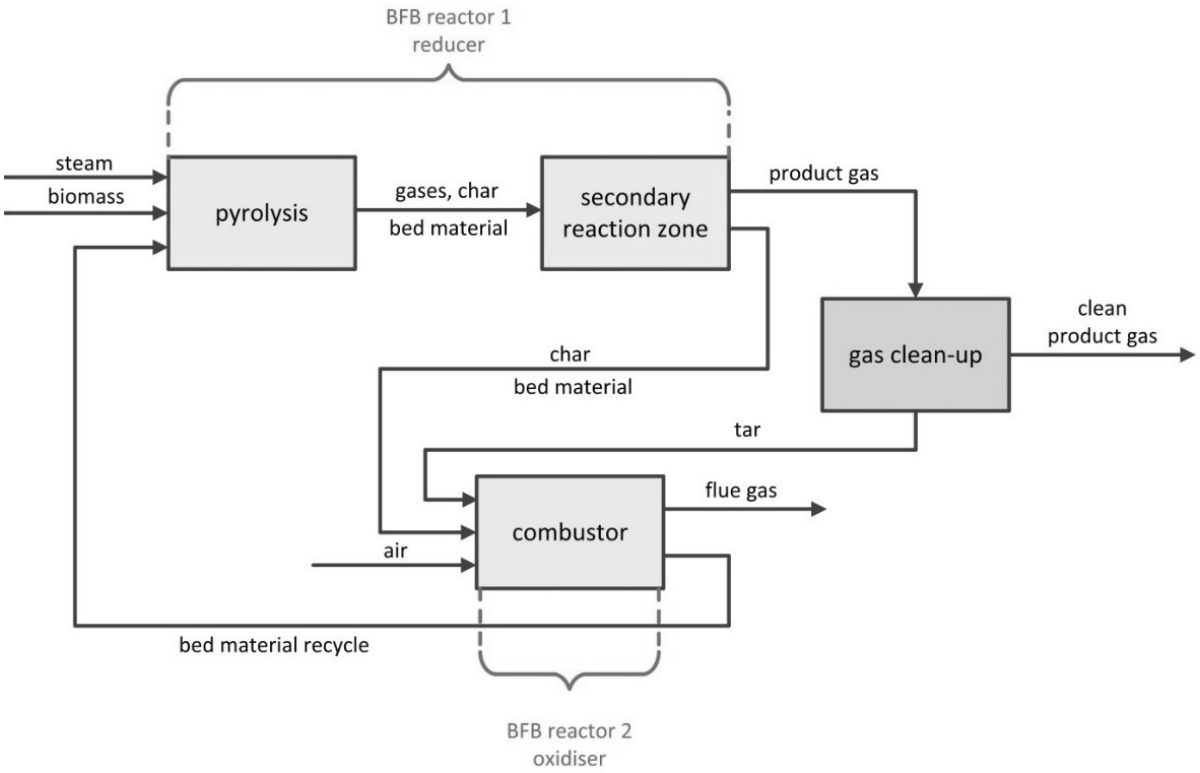

Fig. 4. Model of chemical looping combustion for biomass gasification utilizing two bubbling fluidized beds.

2.3.2. Combustor

In the combustor, the second bubbling fluidized bed, air is provided and the char and tar are burned in an exothermic reaction. The heat produced in this reaction is absorbed by the bed material which circulates between the two reactors. If the excess heat of the combustor is exactly the amount of heat necessary for the gasifier, the whole process can be run autothermically. This reactor is also referred to as the air reactor.

2.4. The MILENA reactor

A pilot plant using the previously mentioned technology is scheduled to be built in 2015, by the Energieonderzoek Centrum Nederland, the ECN [8]. This plant will use the MILENA gasification process, which is an indirectly circulating fluidized bed gasification technology [8]. The gasifier consists of three parts, the gasifier riser, the settling chamber and the downcomer. The combustion section only consists of one part. Biomass is fed into the gasifier riser with some superheated steam. The biomass is heated to 850 °C by the bed material in the gasifier section. The heated biomass is then converted into gas, char and tar, and the tar is then reformed into more product gas. The downcomer transports the bed material and char into the combustor. The combustor operates as a bubbling fluidized bed. In the BFB, there is an excess of steam for tar reforming and the contact with the bed material is better. Olivine is used as a catalytic bed material. The producer gas leaves the reactor from the top and it is sent to the cooling and gas cleaning section. The typical residence time of gases is several seconds.

2.5. The TNEE reactor

In this project, the TNEE gasifier is used as a case study in the modeling of indirect biomass gasification. It was developed by the Tunzini Nessi Equipment Companies [1]. The gasifier consists of the same three parts as the MILENA reactor but in contrast to the MILENA, the gasifier is not a riser but a bubbling fluidized bed while the combustor is a high velocity riser. This makes the residence time in the gasifier longer. Steam is not the fluidization gas, but 14 % of the production gas is recycled for fluidization. The bed is operated at a relatively low temperature of 760 °C. The solid circulation material is transported from the dense phase to the combustor where the produced char is burned. This exothermic reaction heats up the solids after which they are fed to the gasifier at the top of the reactor. This means that the freeboard has a higher temperature than the dense bed. About 5 % of the char is entrained from the dense bed to the freeboard.

2.6. Tars produced in biomass gasification

Eliminating the tars produced in biomass gasification is a key aspect in obtaining a technically feasible, advanced gasification process [13]. Tars can condense and foul the reactors, but when they are gasified and eliminated, a higher amount of product gas can be yielded. Tar is an extremely complex mixture of organic compounds that is produced during thermochemical conversion processes of organic materials and because of its complexity, no consistent definition for tar can be given [14]. Some definitions state that all hydrocarbons with a molecular weight higher than benzene are defined as tar [15]. The tar composition changes depending on the composition and type of biomass that is used. The tar mixture includes single and multiple ring aromatic compounds along with other oxygen containing hydrocarbons. Much research has been done to identify all tar components and the inter-connections between them [16]. There are a couple of classifications which are often used to divide the different tar components. First the tar classification by Milne et al. [17], where tars are divided into four groups, namely the primary products, which are cellulose-derived, hemicellulose-derived and lignin-derived products. The second group are the secondary products, characterized by phenolics and olefins, the third group are derivatives of aromatic compounds and the fourth group are condensed tertiary products which are polycyclic aromatic hydrocarbons. Primary products are destroyed before the tertiary products appear. A second classification method is to divide the tars into six lumps [18], which are benzene, 1-ring compound, naphthalene, 2-ring compounds, 3- and 4-ring compounds and phenolic compounds.

3. Oxygen carriers as bed material

Typically, the bed material used for indirect biomass gasification is inert sand, which only plays a role as a heat transfer agent. But in chemical looping combustion, the oxygen needed for the combustion of fuels is provided by oxygen carriers. These are metal oxides that have sufficient mechanical properties for looping, they can easily be oxidized and reduced and they have high reactivity with the hydrocarbons that need to be combusted. Using the correct oxygen carriers in biomass gasification can reduce the amount of tar produced and produce enough heat in the fuel reactor to heat up the endothermic air reactor. There are many oxygen carriers that are suitable for these purposes, but very limited kinetic data is available.

The active bed materials for the oxygen transport that will be considered for the biomass gasification process are ilmenite and olivine. Ilmenite is a titanium-iron oxide mineral with the idealized formula $FeTiO_3$. Olivine, a magnesium iron silicate with the formula $(Mg,Fe)_2SiO_4$ with different ratios of Mg and Fe. Both materials are common minerals in the Earth's subsurface. Because of their availability, they are a cheap option as fluidized bed oxygen carriers. From literature, it is known that the replacement of sand with oxygen carrier can increase the gas production and can cause high reduction of tar content [6]. When an oxygen carrier is used, more heat will be produced in the combustor and this can make autothermal operation possible.

The formation of tar in the biomass gasification process is an important issue because tar can easily condense which leads to fouling of the reactor and downstream equipment [19]. For tar removal, multiple cleaning technologies have been developed, amongst which hot gas conditioning by catalytic reforming. Different catalysts have been tested, but nickel-based catalysts became the most widely used. In the chemical looping process, the direct contact between fuel and air is avoided and a solid carrier, normally a metal oxide, transports the oxygen between the reactors. CO and H_2 are the most desired products, which are produced by the partial oxidation and steam reforming of hydrocarbon fuels. Chemical looping combustion technology offers a way to clean the tar in a way that will both preserve energy and prevent clogging of the reactor. Catalytic reforming can be done in a temperature range similar to that of gasification, but the major drawback is that catalysts are sensitive to poisoning by carbon deposition. The heavier gas compounds that are formed can be oxidized or reformed by circulating oxygen carriers in the form of metal oxides [19]. The deactivated metal oxides will be recirculated to the air reactor, where the deposited carbon is combusted and the metal oxides are reoxidized.

In literature dolomite and olivine are both considered as a tar reducing bed material for biomass gasification [20]. The combination of magnesium-oxide and calcium-oxide, present in calcined dolomite, has been shown to have better activity towards tar reduction compared to its constituents separately [21] [22]. Dolomite is believed to have a slightly higher activity, but olivine has a higher attrition resistance. This makes it a better prospective candidate for use as a bed material in fluidized beds [16]. However, in literature not much is known about the kinetics of tar reduction reactions with olivine. Only kinetics with a nickel-olivine catalyst are found [23].

Ilmenite is a well-known oxygen carrier, but not much has been documented about the use of ilmenite in biomass gasification. Min et al. [24] describe ilmenite as a catalyst for the steam reforming of tar from the pyrolysis of mallee woody biomass. Ilmenite is said to have a high and consistent activity for both small and large aromatic ring systems [24].

To verify the limited kinetic information found in literature for the steam reforming of tar by ilmenite and olivine, kinetic experiments are done. These experiments are elaborated upon in the experimental section of this report.

4. Project outline

A large amount of experimental work has been done on biomass gasification, while the work on modeling of indirect gasification in two fluidized beds using an oxygen carrier is still limited. Besides that, there is some literature about the abilities of oxygen carriers to reduce the tar concentration in the biomass gasification process [19], but no theoretical work has been drawn up yet. A model for indirect biomass gasification is needed that includes active bed material for tar steam reforming. With such a model, multiple different oxygen carriers could even be investigated in terms of efficiency for the tar conversion process for scale up as well as process optimization.

The main goal of this project is the development of a phenomenological model for indirect biomass gasification using oxygen carriers as bed material for the optimal production of syngas. Furthermore, experimental work is done to study the efficiency of two oxygen carriers for tar reduction, olivine and ilmenite. The knowledge gained in the experimental work is then applied to the theoretical model to optimize the indirect gasification process.

To get more insight into tar reduction in the presence of an oxygen carrier, experiments in a gas-solid reactor will be set up. Because there are many different tar compositions, they cannot all be investigated. Only toluene will be used as a model tar component. It represents a stable aromatic structure apparent in tar formed with high-temperature processes, and it is one of the major tar species [17]. For a better understanding of tar destruction, toluene steam reforming was chosen as a model reaction.

The functionality of the oxygen carriers will be tested in a packed bed reactor with a gasified mixture of water and toluene, the model tar component. Both ilmenite and olivine will be used as oxygen carriers because of their low costs and their availability. Some kinetic information about toluene steam reforming with a nickel olivine catalyst [3] [23] will be compared to the data from the experiments. The temperature, at which the experiments for the tar steam reforming are executed, will be determined by testing at the optimal conditions for syngas production.

The oxygen carriers will be tested for reactivity to the possible side reactions that could be present in the reactor. The methanation reaction, the steam methane reforming reaction and the water-gas shift reaction will be evaluated in the presence of the catalysts and the results will be compared to blank tests. The same temperature as in the toluene steam reforming will be used.

The model for biomass gasification will be developed in Aspen plus. So far, an initial TNEE model in Aspen Plus with sand as bed material has been set-up in a prior graduation project [2] . In this project that model will be extended to support kinetics of different oxygen carriers and to get a better understanding of the impact of the use of an oxygen carrier in the overall process. The kinetics of the toluene steam reforming are obtained from open literature and verified by the experiments in the packed bed reactor. Finally, the kinetics will be implemented in the Aspen Plus model to assess the impact of the use of an oxygen carrier in the overall process performance.

5. Oxygen carriers

The properties of the two oxygen carriers are compared in this section. The goal is to determine to what extent their structural differences influence the catalytic effect of olivine and ilmenite on the steam tar reforming reaction.

5.1. Structures and composition

Olivine

Olivine is a magnesium iron silicate with the idealized formula $(Mg,Fe)_2SiO_4$. The ratio of magnesium and iron can vary between the two endmembers of the solid solution series of forsterite (Mg_2SiO_4) and fayalite (Fe_2SiO_4). Olivine can incorporate minor amounts of manganese and nickel. The crystal structure of olivine includes aspects of the orthorhombic P Bravais lattice, which can be seen in figure 5. It arises when each silica unit is being joined by metal divalent cations where every oxygen atom in SiO_4 binds to 3 metal ions [25]. In table 1 below, the composition of Austrian olivine in mass percentages is given [26].

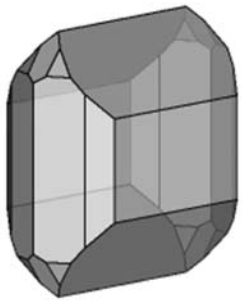

Fig. 5. Orthorhombic crystal structure of olivine.

Table 1. Atomic composition of olivine.

Atom	Composition (wt%)
Magnesium (Mg)	21.2
Iron (Fe)	5.2
Silicon (Si)	16.5
Oxygen (O)	14.6
Nickel (Ni)	0.1
Aluminium (Al)	0.4
Chromium (Cr)	0.3
Calcium (Ca)	0.7
Manganese (Mn)	0.1

Table 2. Atomic composition of ilmenite.

Atom	Composition (wt%)
Titanium (Ti)	36
Iron (Fe)	23
Oxygen (O)	40
Magnesium (Mg)	0.2
Aluminium (Al)	0.5
Potassium (K)	<0.01
Sodium (Na)	<0.01
Calcium (Ca)	<0.01
Silicon (Si)	<0.01

Ilmenite

Ilmenite is a titanium-iron oxide mineral that has the idealized formula $FeTiO_3$. It can be gained from ilmenite placer deposits and ilmenite sands and it can easily be processed. Ilmenite is the main starting material for titanium dioxide pigments as it contains up to 53 % TiO_2 [27]. Ilmenite often contains small quantities of magnesium and manganese. It can form a solid solution with magnesian and manganiferious endmembers of the solid solutions geikielite (MgTiO3) and pyrophanite ($MnTiO_3$). The composition of most ilmenites however, stays close to the idealized formula. The composition of Norwegian ilmenite in mass percentages is given in table 2 [24]. Ilmenite crystallizes in the trigonal system, which can be seen in figure 6, and its structure consists of an ordered derivative of the corundum structure.

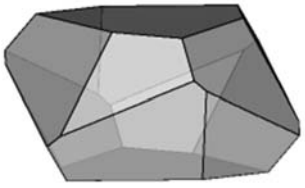

Fig. 6. Trigonal crystal structure of ilmenite.

5.2. Properties

The olivine used in this work is natural olivine from Magnolithe GmbH, the properties of this olivine are well known and documented [28] [29]. The properties of olivine are shown in table 3. In comparison to other natural materials as dolomite, olivine has a good attrition resistance which makes it suitable for use as a bed material in fluidized beds [16].

Norwegian ilmenite was used in experiments. The same Norwegian ilmenite has been analyzed in literature [30]. It was assumed that the properties for the used ilmenite are similar. The properties of ilmenite are shown in table 4. Ilmenite is somewhat more brittle than olivine, but still well suitable for use in fluidized beds. Its BET surface is higher than the BET surface of olivine, which means the amount of physical adsorption of gas molecules on its solid surface, is higher, which leads to faster catalytic reactions.

Table 3. Properties of the oxygen carrier olivine.

Property	Olivine
XRD	$MgSiO_3$, Fe_3O_4, $MgFe_2O_4$
True density (kg/m^3)	3320
BET surface (m^2/g)	0.18
Mohs scale of hardness	6.75
Molar mass (kg/mol)	0.1533

Table 4. Properties of the oxygen carrier ilmenite.

Property	Ilmenite
XRD	Fe_2TiO_5, Fe_2O_3, Fe_3O_4, TiO_2
True density (kg/m^3)	4250
Porosity (%)	35
BET surface (m^2/g)	0.4
Crushing strength (N)	1.0
Mohs scale of hardness	5.25
Molar mass (kg/mol)	0.1517

5.3. Use in chemical looping

Olivine

Olivine is seen as an attractive active bed material for chemical looping combustion. The iron oxide available in olivine can transfer oxygen to the gasification reactor [31]. Olivine is said to increase the CH_4 conversion. Combination of olivine with other natural minerals such as ilmenite can improve the hydrocarbon conversion moderately, especially for fuels with low gaseous hydrocarbon contents like gasification of product gas or solid fuels [31].

Oxygen carrier capabilities of olivine in a chemical looping gasification process are quantified in literature by analysis of reduction and oxidation cycles, carried out in a thermogravimetric analyzer (TGA). More information about TGA analysis can be found in appendix 11.1.1. The TGA results, according to Lancee et al. [32] indicate that a minimum of 18 % of the iron, present in olivine is capable of transferring oxygen on a timescale of minutes. Almost half (44 % to 51 %) of the iron in olivine from Magnolithe exists in the form of free iron oxide phases [32].

When reduced, part of the iron oxide phases reduce to metallic phases, but a small fraction is reintegrated in the Fe^{2+} phase of olivine. Olivine can transport 0.5 wt% of oxygen and the material oxidizes and reduces on two different time scales. The fast process is attributed to surface oxidation and reduction [32]. Oxidation of olivine causes an iron enriched layer to form at the surface of the particles. This is a reversible process as the thickness of this layer decreases when olivine is reduced. The structural change in olivine occurs in two different time scales as well. In the fast process, the surface is enriched with iron at the expense of silicon, to oxidation of near surface iron. In the slower process, iron and oxygen enrichment occurs at the expense of silicon and magnesium is caused by migration of those elements through the material [32]. The oxygen transport capability of olivine is heavily dependent on the composition of olivine, especially in the near surface region [32].

Olivine can be used as a primary catalyst for tar destruction of in indirect biomass gasification [22]. It can remove a large fraction of the tar produced after the pyrolysis of biomass, however the product gas will not completely be cleared of tar as it leaves the gasification reactor. Catalytic properties of olivine are heavily dependent on the thermodynamics, mainly the gas composition and temperature in the gasifier. This influences the chemical state of the iron at the surface of the olivine particles [29]. It is stated that olivine has a strong catalytic effect on steam reforming of tars and this is improved by the presence of H_2 [29].

Ilmenite

Ilmenite is seen as a low cost and promising material for use on a large scale in chemical looping combustion processes. After activation with air, the ilmenite particles form an external shell, enriched with iron [33]. The reactivity increases with activation of ilmenite at higher temperatures, but the oxygen transport capabilities decrease. Ilmenite has low attrition values during fluidized-bed operation and no defluidization occurs for typical operating conditions in a CLC process [33].

To determine the oxygen carrier capabilities of ilmenite in a chemical looping combustion process, reduction and oxidation cycles carried out in a TGA are compared in literature [33]. For the reducing gases, H_2, CO and CH_4 are used. O_2 is used for the oxidation step. The reactivity of ilmenite is tested with various fuels in a CLC system. Ilmenite can transport up to 4.0 wt% of oxygen [33]. The activated ilmenite exhibited high reactivity in both reduction and oxidation reactions, with times for complete conversion at 950 ℃ lower than 120 seconds using 15 % of H_2, CO or CH_4, and 30 seconds using 21 % of O_2 [34]. The oxidation and reduction of ilmenite proceed between the reduced form ilmenite, $FeTiO_3$ and the oxidized form Fe_2TiO_5 + TiO_2 with the likely intermediate Fe_2O_3 or Fe_2O_3•TiO_2 [35]. Other intermediates may be possible as well. It seems like ilmenite is a faster and better oxygen carrier than olivine, which can be explained by its higher iron content and a possible difference in iron mobility throughout the material.

Activation remains crucial in the activity of ilmenite [30]. It has a beneficial and strong influence on the solids inventory needed in both the air and the fuel reactor of the chemical-looping system. Ilmenite shows no tendency of decreased reactivity after multiple oxidation and reduction cycles [30]. Its low cost, moderated solids inventory and oxygen transport capability make ilmenite a suitable compound for solid fuels combustion in a CLC system [30].

Ilmenite exhibits high and consistent activity for the steam reforming of tar into gases due to its highly dispersed iron-containing species [24]. This has been tested in a furnace with temperatures ranging between 500 ℃ and 850 ℃ for small and large aromatic ring systems in biomass volatiles [24]. After reaction, ilmenite was analyzed by XRD to determine the change in iron species. Extra steam in the biomass gasification process plays an important role in the minimization of coke formation on the catalyst surface in the fluidization zone. Minimizing the coke formation is important to ensure available catalyst surface for reaction, which leads to more tar destruction [24].

5.4. Catalytic tar decomposition

According to Nitsch et al. [36], the H_2O concentration in the reactor is one of the most important parameters in the catalytic activity of oxygen carriers. Experiments and characterizations indicate that a high concentration of H_2O in the reactor oxidizes the catalyst and hinders catalytic activity. Low concentration gives reduced active sites and a high activity in steam reforming of tars. Without any water, oxygen carriers are still catalytically active, but steam reforming is then impossible. This causes tars to polymerize at the catalyst surface. Without a catalyst, steam reforming of tars remains extremely low at 850 °C.

A mechanism proposed for catalytic decomposition of tars over an iron catalyst is proposed by Uddin et al. [37] and is shown in figure 7. Olivine and ilmenite behave like the iron catalysts described. The derived carbon Iron oxide in the form Fe_2O_3 transfers to Fe_3O_4 during the gasification reaction. This form has catalytic activity for tar reforming. The state of the iron at the surface area of the iron oxide catalyst thus plays a major role in the catalytic tar reduction. Tar can absorb dissociatively on the iron oxide surface [38] [39]. The surface iron connected to Fe_3O_4 then reacts with tar by oxidation with labile O and/or –OH species [40]. This produces CH_4, C_2H_4, H_2O, CO and H_2 in the first stage of the reaction over the iron oxide catalyst. Water-gas shift occurs over the iron oxide active site and converts CO and water into more CO_2 and H_2. This site is different than the active site for tar decomposition.

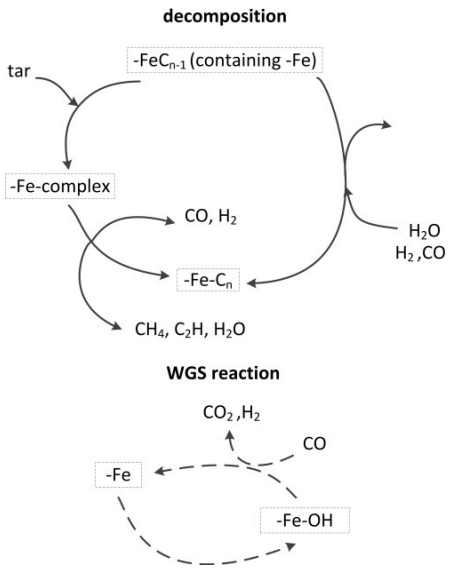

Fig. 7. Mechanism of catalytic decomposition of tars over an iron oxide catalyst [37].

The catalytic tar destruction mechanism depends on more factors than the iron content alone. The other compounds in the oxygen carrier and their mobility play an important role as well. To determine the tar reforming capabilities of the oxygen carriers, experiments need to be done in which the amount of tar decomposed and the gas production at the outlet can be quantified.

5.5. Reactions catalyzed by oxygen carriers

For a better understanding of tar destruction, toluene steam reforming was chosen as a model reaction, taken from literature by Swierczynski et al. [3]. The reaction described in [3] is catalyzed by olivine doped with nickel. Only toluene was used as a model tar component as it represents a stable aromatic structure apparent in tar formed with high-temperature processes, being one of the major tar species [17]. The simplified reactions predicted, including water-gas shift, are shown in figure 8.

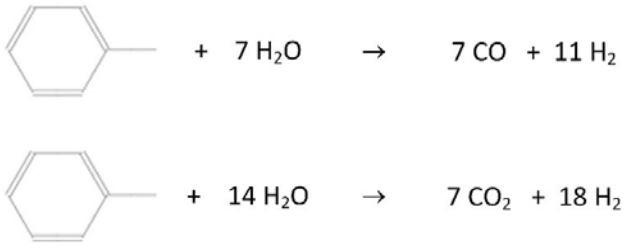

Fig. 8. Toluene steam reforming reactions [3].

Besides the simplified reactions, other tar decomposition reactions for toluene can occur. A list of all possible reactions is given in table 5 [41].

Table 5. Potential tar decomposing reactions in the presence of an oxygen carrier.

Nr.	Reaction	Equation
1	Steam reforming	$C_nH_m + n\,H_2O \rightarrow n\,CO + (n + 0.5\,m)\,H_2$
2	Steam dealkylation	$C_nH_m + x\,H_2O \rightarrow C_iH_j + p\,H_2 + q\,CO$
3	Hydro cracking	$C_nH_m + (n \cdot 2 - (m/2))\,H_2 \rightarrow n\,CH_4$
4	Hydro dealkylation	$C_nH_m + x\,H_2 \rightarrow C_iH_j + q\,CH_4$
5	Dry reforming	$C_nH_m + n\,CO_2 \rightarrow 2n\,CO + 0.5\,m\,H_2$

When the toluene molecules are decomposed, new gas molecules are formed which are taking part in equilibrium reactions. These reactions are shown in table 6. To test the catalytic effect of the oxygen carriers on these reactions, gas phase experiments need to be done.

Table 6. Potential gas reactions in the presence of an oxygen carrier.

Nr.	Reaction	Equation
1	Methanation Steam methane reforming	$CO + 3\,H_2 \rightleftarrows CH_4 + H_2O$
2	Water-gas shift	$CO + H_2O \rightleftarrows H_2 + CO_2$
3	Carbon methanation	$2\,H_2 + C \rightleftarrows CH_4$
4	Water gas reaction (1)	$CO + H_2 \rightleftarrows H_2O + C$
5	Water gas reaction (2)	$CO_2 + 2\,H_2 \rightleftarrows 2\,H_2O + C$
6	Boudouard reaction	$2\,CO \rightleftarrows CO_2 + C$

6. Experimental analysis of oxygen carrier activity

The phenomenological model needs reliable kinetic data for the decomposition of tar in the presence of oxygen carriers. In literature, a model of kinetics for olivine, doped with nickel, was found [23]. Experiments with the oxygen carriers olivine and ilmenite were done and the gathered data is compared to the kinetic data in literature. The particle size of olivine and ilmenite is determined to ensure that the comparison of the two oxygen carriers is accurate. This data can be found in appendix 11.2. The average particle size of olivine was 526 µm and the average particle size of ilmenite was 342 µm. These sizes are similar enough for comparison in a packed bed reactor.

In a prior graduation project, ilmenite activity with toluene was tested in the TGA. [2] The results were not comparable to results found in open literature, which led to the recommendation that a gas chromatography analysis has to be added. This will help to gain insight in the reactions occurring in the presence of an oxygen carrier. Tests in a packed bed reactor were done. The reactions mentioned in the section 5.5 were investigated. First, blank tests were done without an oxygen carrier, than toluene steam reforming with ilmenite and olivine was tested and finally the activity of olivine and ilmenite in gas reactions was tested.

6.1. Experimental setup

The experimental set-up used in this work is shown in figure 9. This packed bed reactor consists of a quarts tube with quarts particles to assure good gas mixing of the reactants. The active bed is about 3 cm of bed material mixed with quarts particles of the same particle size. The inlet of the quarts tube is connected to mass flow controllers where different gases can be supplied into the reactor. The controlled evaporation and mixing equipment (CEM) is used to vaporize compounds that are liquid at room temperature. The outlet of the reactor is cooled down and the gas fraction can be analyzed. The liquid fraction is condensed in two coolers in series to avoid any liquid to flow into the gas analyzer. At the bottom of the cooler a purge valve is installed it to allow the tapping the condensed liquid, which is analyzed by gas chromatography. The temperature is measured in two different points in the bed material to ensure the absence of temperature profiles during experiments.

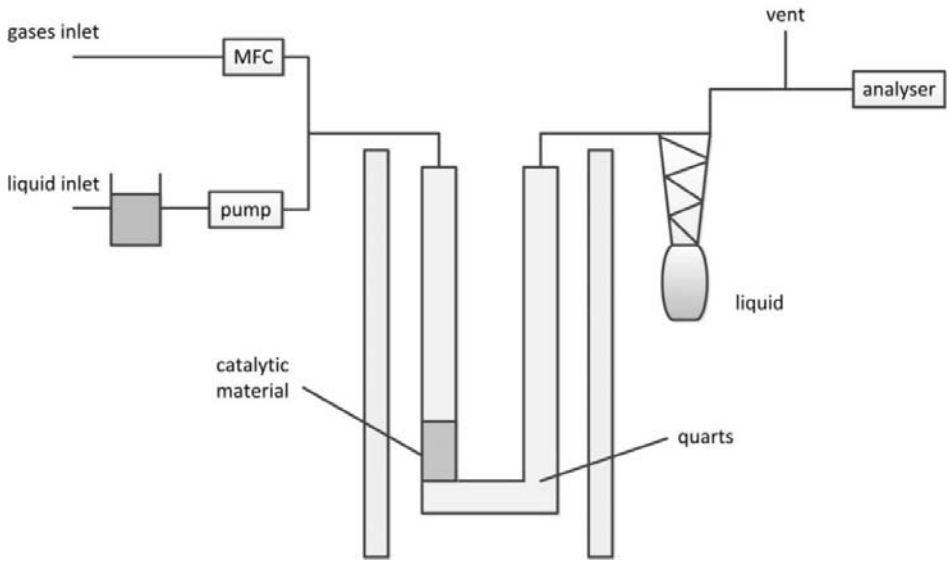

Fig. 9. Schematic overview of the experimental kinetics set-up.

6.2. Blank experiments

Blank tests were done to determine if there is interaction between the gases in the system without a catalyst. The toluene steam reforming reaction and gas reactions, mentioned in section 5.5, were tested. These experiments were done with an empty reactor.

6.2.1. Toluene steam reforming

To determine the interaction between toluene and water at a high temperature without a catalyst, blank tests were done at various temperatures that are normally used for gasification in industry. All experiments were done at atmospheric pressure. In these experiments, an empty reactor was attached to the kinetics set-up and toluene and water, which were both vaporized with nitrogen, were flushed through the reactor. For the blank tests, only temperatures above 800 ℃ were used, to determine when thermal cracking begins to play a role. It is stated that reaction temperatures above 650 °C will not yield unwanted side products [23]. However, thermal cracking is not mentioned. The results of the blank tests done for the water-toluene system are shown in table X below. These inlet concentrations were chosen within the limits of the gas analyzer. Volume concentrations below 0.1 % cannot be detected by the analyzer.

Table 7. Blank experiments done with toluene and water in the kinetics set-up.

Temperature in the reactor	Inlet gases	Gas production
800 °C	0.15 l/min N_2, 0.5 g/min H_2O, 0.1 g/min C_7H_8	No reaction
940 °C	0.15 l/min N_2, 0.5 g/min H_2O, 0.1 g/min C_7H_8	Reaction
850 °C	0.15 l/min N_2, 0.5 g/min H_2O, 0.1 g/min C_7H_8	No reaction

At 800 °C, no gas production was observed, and the condensed samples only contained water and toluene. No thermal cracking or reactions between water and toluene occurred at this temperature. At 940 ℃ however, small amounts of gas production (CO, H_2 and CH_4) were observed, most likely caused by thermal cracking of toluene. The liquid condensed samples were analyzed with GC-MS to determine the products that were formed.

The condensed samples taken at 940 ℃ in the reactor were analyzed with GC-MS. This is an analytical technique that combines gas chromatography with mass spectrometry. More information about GC-MS can be found in appendix 11.1.3. The spectrum of the 940 ℃ sample is shown in figure 10.

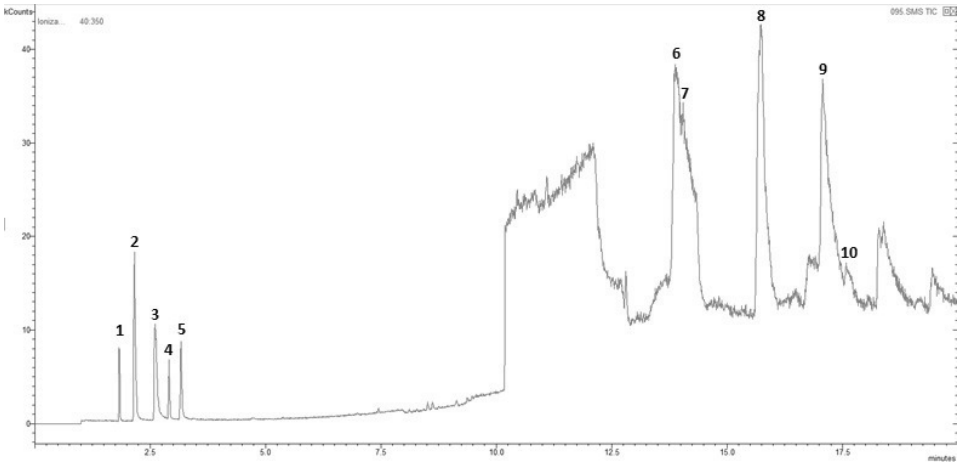

Fig. 10. GC-MS spectrum of the condensed sample of the blank test at 940 ℃.

Table 8. Probability of molecules in the sample of the blank test at 940 ℃, based on the peaks measured by the GC-MS.

Peak	Proposed molecules	Formula	Probability (%)
1	Phenylglyoxal	C8H6O2	7.33
2	Phenol	C6H6O	20.70
3	Benzyl alcohol	C7H8O	31.61
4a	3-methylphenol	C7H8O	49.11
4b	2-methylphenol	C7H8O	22.37
4c	4-methylphenol	C7H8O	12.88
5a	3-methylphenol	C7H8O	41.23
5b	4-methylphenol	C7H8O	34.83
5c	2-methylphenol	C7H8O	8.74

Peak 6 until 10 are higher mass components with a large uncertainty. It might even be possible that some silica of the glassware was dissolved at this temperature and incorporated in molecules. Alternatively, the silica can be from the column of the GC-MS itself.

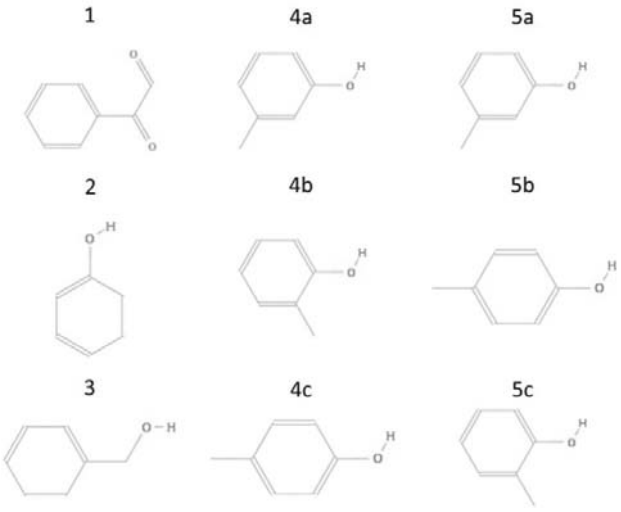

Fig. 11. Molecules produced in the blank sample at 940 °C, measured by GC-MS.

Peaks 1 until 5 indicate that at 940 ℃, various molecules were formed when the toluene reacts with hydroxyl radicals [42], which can form in water at higher temperatures. These reactions yield unwanted products, which are corrosive, toxic and carcinogenic. However, in some types of biomass, these compounds are already present. The production of unwanted side products and large amounts of carbon deposition is avoided by limiting the maximum temperature of the reactor at 800 ℃.

To analyze when gas production starts, the temperature was slowly increased from a starting point of 800 ℃ to the point where gas production, and thus thermal cracking, starts. At 850 ℃, traces of gas production started, which indicates that during the gas experiments, the reactor should not exceed 800 ℃ to ensure that no thermal cracking occurs. After the blank experiments, the reactor used for the experiments was covered with a black deposition, which is most likely carbon deposition formed during thermal cracking.

6.2.2. Gas reactions

The most important gas reactions mentioned in section 5.5 were investigated. These experiments were done with an empty reactor at 800 ℃. The various reactions listed in table 9 were each tested by feeding their respective reactants and measuring the product composition. The feed was adjusted with gas calibrations of the mass flow controllers. The calibration curves are added in appendix 11.3. All experiments were diluted with nitrogen due to the limitations of the gas analyzer.

Table 9. Overview of blank gas experiments.

Nr.	Reaction name	Reaction	Inlet CO (%)	Inlet H_2 (%)	Inlet CH_4 (%)	Inlet H_2O (%)	Inlet N_2 (%)
1	Methanation	$CO + 3\,H_2 \rightleftarrows CH_4 + H_2O$	25	25	0	0	50
2	Steam methane reforming	$CH_4 + H_2O \rightleftarrows CO + 3H_2$	0	0	25	25	50
3	Water-gas shift	$CO + H_2O \rightleftarrows CO_2 + H_2$	30	0	0	30	40

a) Methanation reaction, blank test

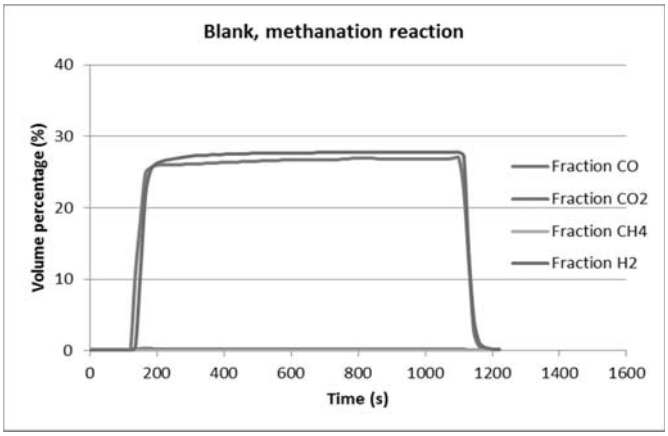

Fig. 12. Blank methanation reaction.

In the blank methanation experiment, the amount of H_2 and CO conformed to similar amounts at the inlet. In figure 12, the inlet concentrations of 25 volume percent can be seen. This means that spontaneously, without catalyst, no methanation occurs at 800 ℃.

b) Methane steam reforming, blank test

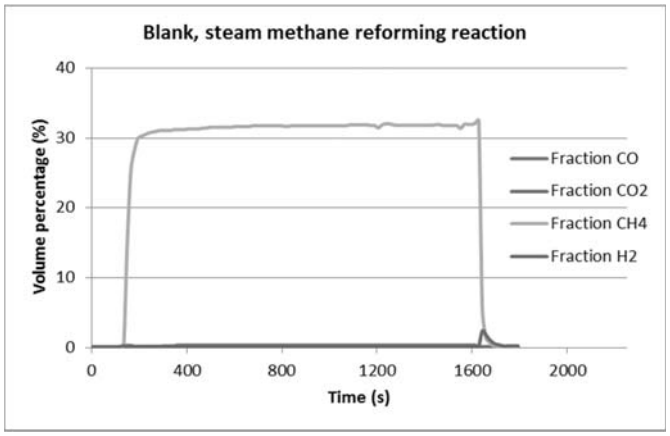

Fig. 13. Blank steam methane reforming reaction.

In figure 13 the results of the blank methane steam reforming test are depicted. Water was condensed before the gas analyzer, the input of 25 % CH_4, 25 % H_2O, and 50% N_2 gives an expected value without reaction of 33 % CH_4 and 67% N_2. This is the average value reached on the analyzer so no steam methane reforming reaction occurs at 800 ℃. The small deviations in the analyzer are consequences of minimal variations in the CEM, the evaporator that vaporizes the water.

c) Water-gas shift reaction, blank test

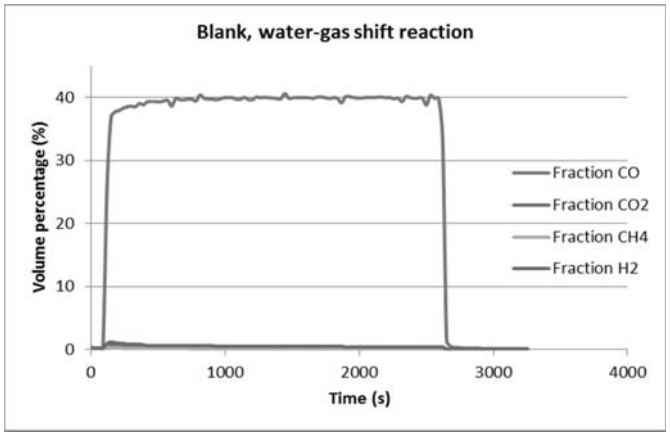

Fig. 14. Blank water-gas shift reaction.

The blank water-gas shift experiment is shown in figure 14. Water was condensed before the gas analyzer, as mentioned for the steam methane reforming reaction. The expected values without water gas shift reaction would be 40 % CO and 60 % N_2. The value of 40% CO could be seen at the outlet. No water-gas shift reaction occurs at 800 ℃. The slight deviations are once again due to the small variations in the vaporization of the CEM.

6.3. Toluene steam reforming reaction experiments with olivine and ilmenite

The toluene steam reforming reaction was executed at various steam to toluene ratios to see the effect on the produced gas. The experiments were all carried out at 800 ℃. The amount of catalytic material used was 1.5 g in all cases. The temperature measured stays constant in both measuring points in the catalytic material which means temperature profiles were absent. Experiments were designed after the work of Swierczynski et al. [3], which uses Ni-olivine as a catalyst. The exact experiments could not be replicated as preliminary testing revealed the limitations of the set-up regarding the low volumetric flowrates used in [3]. The results of a preliminary test can be seen in appendix 11.4. To be able to compare the experiments with [3], the steam to toluene ratio in literature (16 : 1) was kept. In the preliminary experiments, at a ratio of 25 : 1 an optimum was found in the gas production, so this ratio was tested as well. At steam to toluene ratios below 7 : 1, toluene is the limiting component and more methane was produced. These experiments were not further investigated. The experiments of the present work are listed in table 10. Conditions were defined to avoid black material formation on the reactor walls.

Table 10. Gas experiments done at 800 ℃ with olivine and ilmenite in the kinetics set-up.

Nr.	Oxygen carrier	Inlet gases	Steam to toluene ratio
1	Olivine	0.15 l/min N_2, 0.5 g/min H_2O, 0.1 g/min C_7H_8	25 : 1
2		0.15 l/min N_2, 0.44 g/min H_2O, 0.14 g/min C_7H_8	16 : 1
3	Ilmenite	0.15 l/min N_2, 0.5 g/min H_2O, 0.1 g/min C_7H_8	25 : 1
4		0.15 l/min N_2, 0.44 g/min H_2O, 0.14 g/min C_7H_8	16 : 1

a) Steam to toluene ratio of 25 : 1

The gases produced in the presence of olivine are seen in figure 15. About 0.7 % of the toluene at the inlet was converted into product gas, which was calculated with the carbon balance. A small amount of CH_4 was produced, which indicates that the simplified reactions of with Ni-olivine [3] might not be enough to describe the reaction without nickel. It could be that the hydrocracking reaction that yields CH_4 is active as well or there might be other alternatives.

The graph for the toluene steam reforming reaction with ilmenite seen in figure 16 is very different from the one with olivine as an oxygen carrier. It took a large amount of time to reach a steady value in gas production. This is might have been caused by carbon deposition on active sites, the oxidation state of the material or thermodynamics. For the stable part, a higher conversion of toluene was reached than in the olivine experiments. The conversion was about 1.1 %. The ratio between the product gases was comparable to the ratio that can be seen for the olivine experiments. The peak could be caused by competition between several reactions that reaches a steady value after some time.

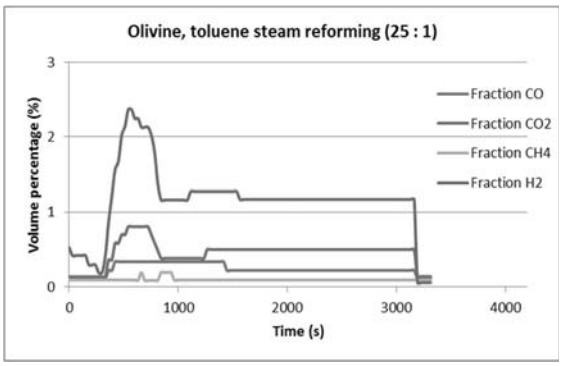

Fig. 15. Olivine toluene steam reforming reaction.

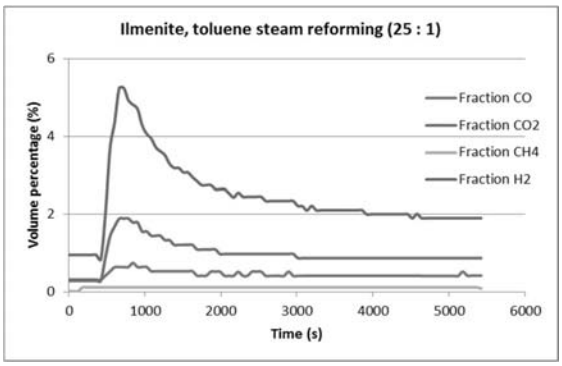

Fig. 16. Ilmenite toluene steam reforming reaction.

The liquid which was condensed before the gas analyzer was collected analyzed by GC, information about the GC is provided in appendix 11.1.1. In the GC, reference toluene and benzene peaks were used to detect how much toluene was left in the sample and if any benzene or other tar components have formed. The GC calculations and spectra have been added in appendix 11.5.

The liquid collected from the kinetics set-up for both olivine and ilmenite showed two phase systems. An example can be seen in figure 17. The top layer has an oil-like appearance. Both phases were measured separately in the GC. The results for olivine are shown in table 11 and the results for ilmenite are shown in table 12. The system was calibrated for toluene and benzene. The top phases contained large amounts of toluene while the bottom phases contained less. In both cases a trace of benzene was present. Less water has been condensed than expected which can be seen in the results of the bottom phase in table 11. This could be caused by several factors. The water could condense less easily than the toluene and be left in the coolers. Water could accumulate in the cooler bends of the kinetic set-up or it could participate in more gas phase reactions such as water-gas shift or reactions with deposited carbon.

Fig. 17. Two phase system collected from the cooler of the experimental set-up.

Table 11. Olivine toluene steam reforming reaction 1 (25 : 1) toluene content.

Phase	Phase volume (mL)	Toluene mass fraction	Toluene mol fraction
1 T	2	0.86	0.87
1 B	35	0.028	0.0021
1 total	37	0.067	0.27

The gas conversion of the toluene steam reforming with olivine was around 0.7 %, so the expected output should resemble the input. Less water was condensed than expected. Because of the peak that can be seen in figure 15 at the start of the experiment, water could be involved in more reactions than toluene steam reforming alone. The reactions reach a steady state after some time. Not many other traces were present in the sample.

Table 12. Ilmenite toluene steam reforming reaction 1 (25 : 1), toluene content.

Phase	Phase volume (mL)	Toluene mass fraction	Toluene mol fraction
1 T	6	0.92	0.81
1 B	34	0.026	0.0020
1 total	40	0.14	0.46

The steam toluene reforming reaction had a conversion of 1.1 %. In comparison to the spectra of the experiments with olivine, many more small peaks could be seen. The GC spectrum can be found in appendix 11.5.3. This is an indication that more different reactions occur than with olivine as an oxygen carrier. To determine what other compounds were formed in the presence of ilmenite, GC-MS was used.

The GC-MS spectrum can be found in figure 18. The peaks are numbered and the compounds including their probabilities are shown in table 13.

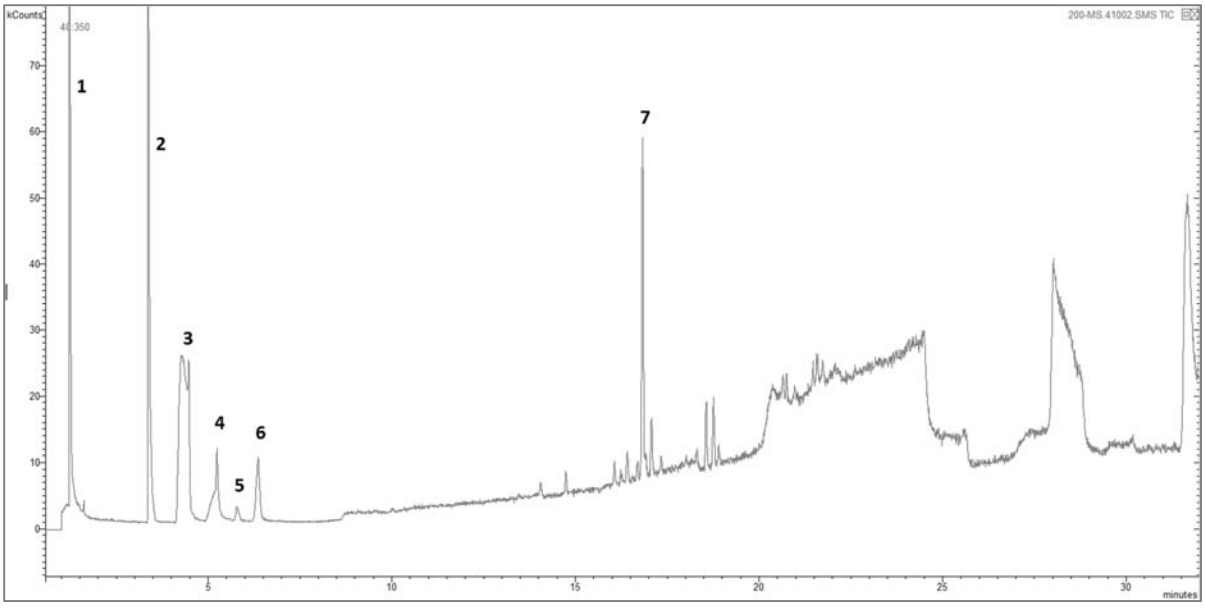

Fig. 18. GC-MS spectrum of toluene steam reforming in the presence of ilmenite (25 : 1).

Table 13. Probability of molecules in the sample of toluene steam reforming with ilmenite, based on the peaks measured by the GC-MS.

Peak	Proposed molecules	Formula	Probability (%)
1	Toluene	C7H8	2.43
2	Phenylglyoxal	C8H6O2	7.28
	2,2-dihydroxy-1-phenylethanone	C8H6O3	3.91
	Benzoylformic acid	C8H6O3	2.91
3	Phenol	C6H6O	32.57
4	Benzyl alcohol	C7H8O	34.07
5	3,5-bis(4-hydroxyphenyl)-4-pentene-1,2-diol	C17H18O4	7.02
	1,2-diphenyl-1,2,ethanediol	C14H14O2	0.58
6	3-methylphenol	C7H8O	52.87
	4-methylphenol	C7H8O	30.45
	2-methylphenol	C7H8O	6.94
7	Bibenzyl	C14H14	24.49

Toluene steam reforming with ilmenite yielded more different kinds of tar than the reaction with olivine. Both the toxic phenol and different methyl phenols were present in the condensate, even though it was in a small amount. Ring polymerization reactions might have occurred, proven by the presence of compounds as bibenzyl, 3,5-bis(4-hydroxyphenyl)-4-pentene-1,2-diol and 1,2-diphenyl-1,2,ethanediol. Polymerization was predicted as a possible tar reaction in literature [24]. As the main goal of these experiments was to eliminate tar, tar polymerization must definitely be avoided.

b) Steam to toluene ratio of 16 : 1

For olivine, the results of the toluene steam reforming reaction with a steam to toluene ratio of 16 : 1 can be seen in figure 19. Only a small amount of toluene was converted into product gas. The conversion of toluene was 0.5 %. There was some methane production, but it was very low.

A conversion of 0.8 % was achieved for the toluene steam reforming reaction with ilmenite seen in figure 20. At the start of the experiment a peak and a valley can be seen before a stable gas production value was achieved. This can be caused by different reactions occurring and reaching a stable value. The time it takes to reach a stable value was much less than in the previous experiment. This can be due to a certain state that the catalyst will already be in after the last experiment. No oxidation between the two experiments has been done. This effect should be further investigated.

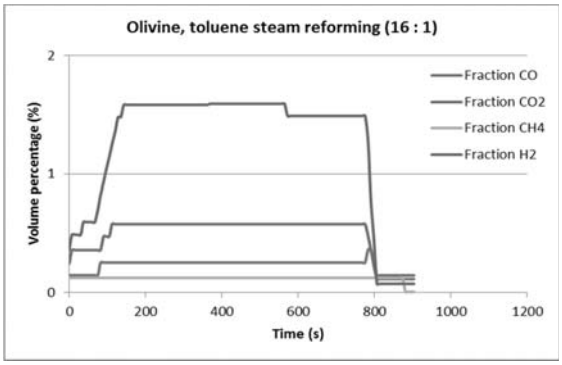

Fig. 19. Olivine toluene steam reforming reaction.

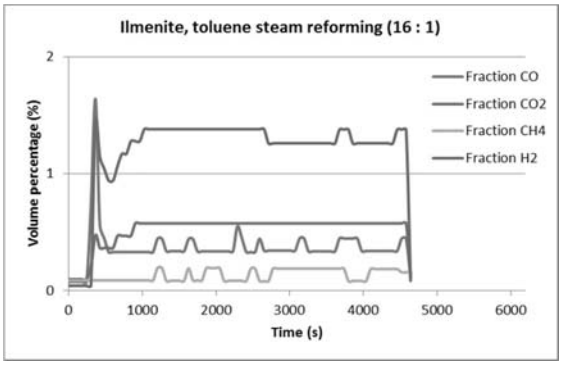

Fig. 20. Ilmenite toluene steam reforming reaction.

The condensed liquid of these experiments were analyzed with the GC. The results were shown in table 14. Only traces of benzene were produced. Not many other small peaks could be seen.

Table 14. Olivine toluene steam reforming reaction 2 (16 : 1), toluene content.

Phase	Phase volume (mL)	Toluene mass fraction	Toluene mol fraction
2 T	6	0.92	0.82
2 B	22	0.026	0.0030
2 total	28	0.19	0.55

In this experiment, the amount of toluene condensed was even larger than for the olivine experiment with a steam to toluene ratio of 25 : 1. More experiments need to be done in order to get more insight in the reliability of the liquid collection. For example at the blank tests with toluene and water, liquid collection can be done in combination with GC analysis.

The concentrations of the liquid condensed in the ilmenite experiment with a steam to toluene ratio of 16 : 1 were not determined by GC as not all of the condensate could be collected. Only the presence of toluene and benzene was examined by GC. The spectrum can be found in appendix 11.5.3. In the sample, toluene and small traces of benzene were present. Other peaks that were observed in the first experiment were present, but they were much smaller. Nevertheless, the sample was investigated with GC-MS. This spectrum can be found in appendix 11.6. The GC-MS confirmed that the same peaks as in the condensate of the first ilmenite experiment were present, but they were much smaller. It can be concluded that this is a direct effect of the steam to toluene ratio. As a very high steam to tar ratio occurs in industry as the amount of tar is minimized. In simulations described in the next section, a ratio of 50 : 1 was used. This ratio could not be achieved with the experimental set-up available.

6.4. Gas reaction experiments with olivine and ilmenite

To see if the two oxygen carriers have catalytic abilities on the reforming of the produced gases, various gas experiments were done at 800 °C. Catalysis of gas reactions can influence the amount of syngas in the product gas of the biomass gasification process. 1.5 g of catalytic material was used. These were compared to the blank tests done in section 6.2.2.

Table 15. Gas experiments done at 800 °C with olivine and ilmenite in the kinetics set-up.

Nr.	Oxygen carrier	Inlet gases	Inlet CO (%)	Inlet H_2 (%)	Inlet CH_4 (%)	Inlet H_2O (%)	Inlet N_2 (%)
1	Olivine	$CO - H_2 - N_2$	25	25	0	0	50
2		$CH_4 - H_2O - N_2$	0	0	25	25	50
3		$CO - H_2O - N_2$	20	30	0	0	50
4	Ilmenite	$CO - H_2 - N_2$	25	25	0	0	50
5		$CH_4 - H_2O - N_2$	0	0	25	25	50
6		$CO - H_2O - N_2$	20	30	0	0	50

The results are shown in the graphs on the next pages. The nitrogen volume percentages are not shown in the graphs.

a) Methanation reaction

The graph of the olivine methanation reaction seen in figure 21, shows a small change in the CO fraction compared to the blank test and the inlet. About 0.5 volume percent of CH_4 was formed, but this does not explain the difference in the CO. H_2 has only changed marginally and not three times the amount of CO which reacted. It might be that CO reacted with the oxygen in the oxygen carrier or the Boudouard reaction occurs, as 1 volume percent of CO_2 was formed as well. There was some gas compression, but it was only minimal. There was a peak at the beginning of the experiment which might be an irregularity of the mass flow controller.

The ilmenite methanation reaction in figure 22 is very similar to the one for olivine. The expected values for CO and H_2 were both 25 %. Like in olivine, a small amount of the CO has reacted with H_2 to form CH_4, which is 0.5 volume percent on average. There was some CO_2 produced as well, which could be caused by water-gas shift of CO and the water, produced by the methanation reaction, or the Boudouard reaction.

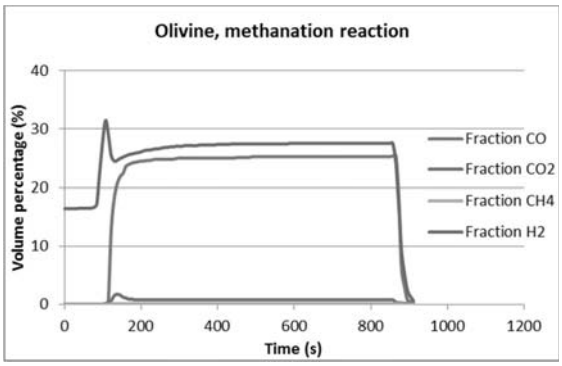

Fig. 21. Olivine methanation reaction.

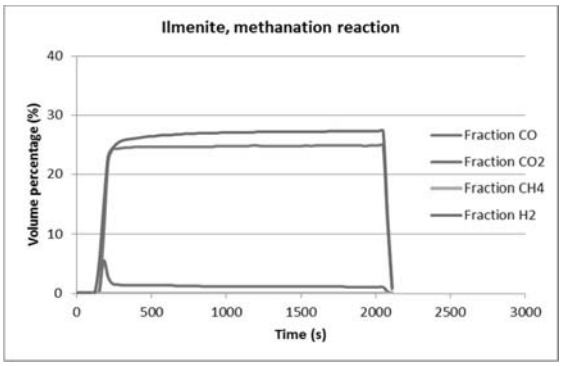

Fig. 22. Ilmenite methanation reaction.

b) Methane steam reforming reaction

As mentioned with the blank tests, water was condensed before the gas analyzer. This means the input of 25 % CH_4 - 25 % H_2O - 50% N_2 gives an expected value without reaction of 33 % CH_4 - 67% N_2. For the methane steam reforming with olivine, this value can be seen on figure 23 and no changes in the gas volume occurred. This means that no methane steam reforming was catalyzed by olivine.

Ilmenite clearly catalyzed the methane steam reforming reaction which can be seen on figure 24. Without reaction of 33 % CH_4 and 67% N_2 would be expected. There is gas expansion. 16 % of H_2 is produced and 7 % of CO No CO_2 is produced, which means that besides methane steam reforming, it might be that other reactions that occurred as well. The results for CH_4 and CO_2 are not shown due to an error in the analyzer. The CH_4 volume percentage should be around 15 %. Ilmenite is said to catalyze the water-gas shift reaction [30] which would lead to some production of CO_2.

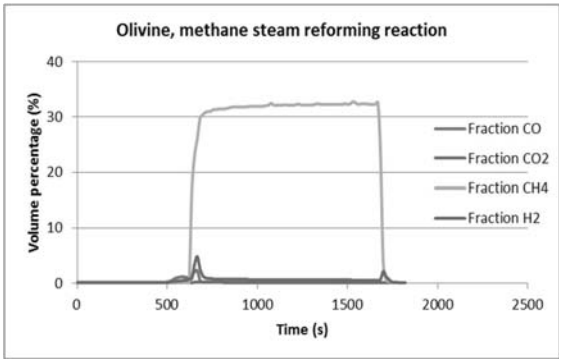

Fig. 23. Olivine methane steam reforming reaction.

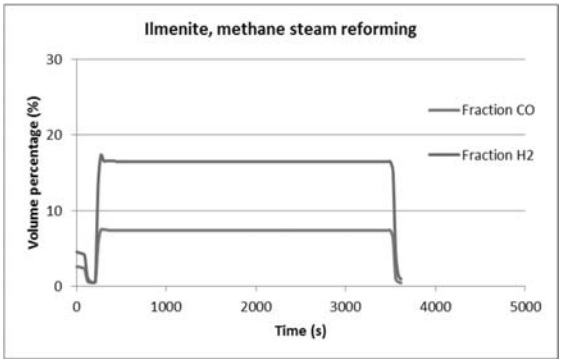

Fig. 24. Ilmenite methane steam reforming reaction.

c) Water-gas shift reaction

Like in the steam methane reforming reaction, water was condensed before the gas analyzer. The expected values without water gas shift reaction would be 40 % CO and 60 % N_2. However, in the graph for water-gas shift with olivine, seen in figure 25, a production of H_2 and CO_2 of around 3 % is clearly seen. This means at 800 °C, olivine catalyzed the water shift reaction to some extent. Around 8 % of the CO available was converted into CO_2 and this was verified in the gas expansion. The exact same amount of H_2 and CO_2 was formed, which indicates that the water-gas shift reaction occurs.

The water-gas shift graph for ilmenite, seen in figure 26, is very different from all the other experiments. The experiment was carried out over a longer period to analyze the effect in time. The production of CO_2 and H2 started slowly, after around 600 seconds. Then, the conversion immediately became larger and a large amount of CO was converted. This effect then became less and less as time passed. No real stable concentration of the gases was found. This effect might be due to carbon deposition. When carbon deposits on the active sites of ilmenite, it blocks the activity for water-gas shift. The carbon balance shows that around 10 % of the carbon at the inlet is lost in carbon deposition. A comparable effect is seen in the toluene steam reforming experiments with ilmenite as well.

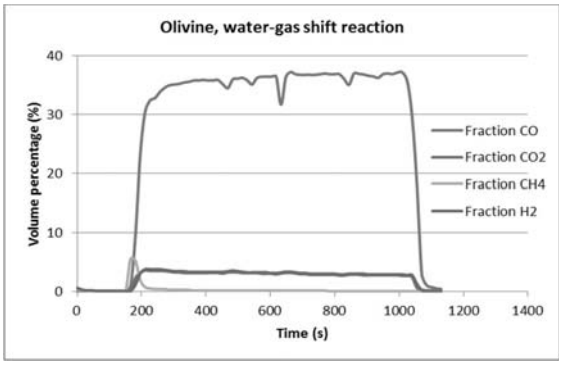

Fig. 25. Olivine water-gas shift reaction.

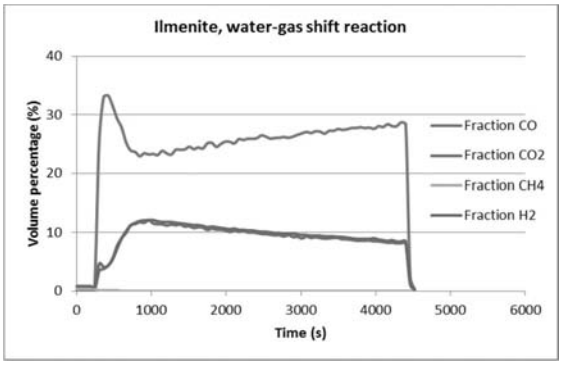

Fig. 26. Ilmenite, water-gas shift reaction.

6.5. Carbon burning experiments

In literature, carbon deposition is reported to occur in the presence of some oxygen carriers, mainly due to the Boudouard reaction ($2\,CO \rightleftarrows C + CO_2$) [19] which was mentioned in section 5.5. It is stated that for ilmenite, the amount of carbon deposition should be very low. After all the gas experiments, so not after the toluene experiments, the reactor was flushed with nitrogen and air to see if carbon deposition had occurred. This was done at a temperature of 800 °C. This experiment was done for the blank test as well, but due to an error in the analyzer, no results could be documented.

a) Carbon deposition burning for olivine

For the burning of carbon deposition on olivine, 250 ml/min air was used, diluted with 2 l/min of N_2. At the beginning of the burning with air, CO, H_2 and CO_2 peaks arise. This indicates that some carbon deposition onto olivine has occurred prior to the burning. If the amount of carbon was estimated with the area under the CO and CO_2 curve and the flow and compared to the overall carbon available in the experiments, the overall deposition was less than 1 %. The small amount of carbon deposition in iron containing oxygen carriers mentioned by Mediara et al [19] is relevant for olivine. The hydrogen peak might be caused by remaining moisture in the cooler parts of the set-up. Water can react with the reduced iron sites on the catalyst material. This is referred to as the steam iron process [43]. As burning occurs, the temperature in the reactor can spike, which results in faster reactions.

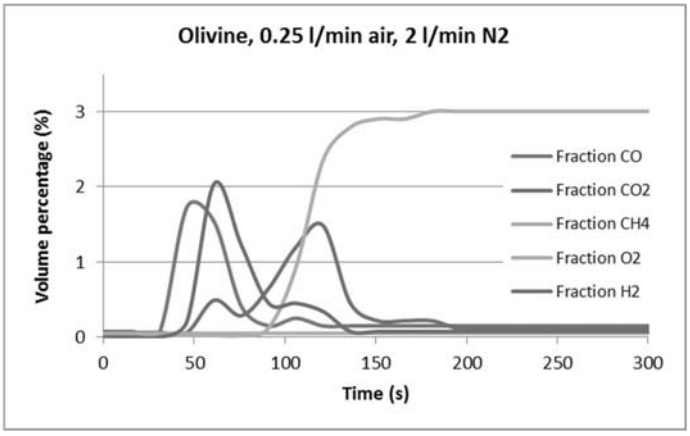

Fig. 27. Carbon deposition detection by burning olivine with air.

b) Carbon deposition burning for ilmenite

The air used in the burning of carbon deposition on ilmenite was undiluted. Nevertheless, the same peaks can be seen. The peaks overlap more, probably because a larger amount of oxygen, relative to the overall volume flow was fed. For ilmenite, the estimation of the carbon deposition was not done. Due to some flawed experiments, no overall carbon inlet can be determined. Still, with the information available of the carbon supplied at the inlet, it can be assumed that it was below 5 %. In the gas experiments, only for water-gas shift, carbon deposition was detected.

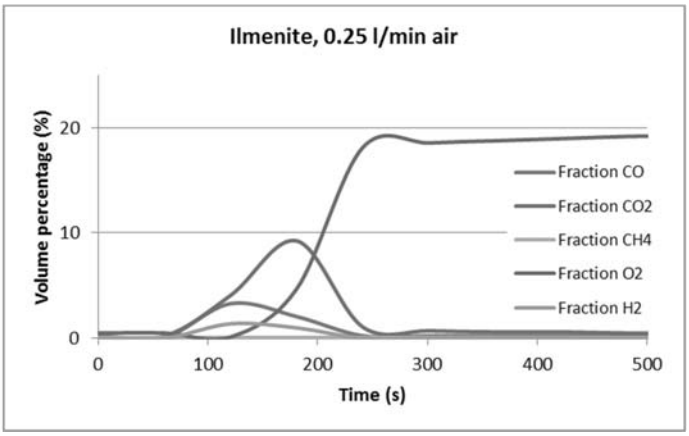

Fig. 28. Carbon deposition detection by burning ilmenite with air.

6.6. SEM and EDX analysis

A SEM or scanning electron microscope was used to analyze the structure of olivine and ilmenite. The local surface composition of the samples was then determined by energy-dispersive X-ray spectroscopy (EDX). More information about these analysis techniques can be found in appendix 11.1.4 and 11.1.5. As an example, one EDX spectrum with the calculations is shown in appendix 11.7. An overview of the analyzed samples is shown in table 16. EDX analysis was only done in one spot due to time limitations, this might not give a good overview of the surface composition of the entire sample.

Table 16. Samples analyzed with SEM and EDX analysis.

Nr.	Oxygen carrier	Samples
1	Olivine	As received (non-activated)
2		After activation with air (1000 °C, 250 ml/min air, 4h)
3		After reaction (800 °C, both toluene steam reforming and gas reactions)
4		After reaction (900 °C, toluene steam reforming reaction)*
5		Reactor wall with deposit (900 °C, toluene steam reforming reaction)*
6	Ilmenite	As received (non-activated)
7		After activation with air (1000 °C, 250 ml/min air, 4h)
8		After reaction (800 °C, both toluene steam reforming and gas reactions, bottom)**
9		After reaction (800 °C, both toluene steam reforming and gas reactions, top)**

* In the preliminary experiments, a temperature of 900 °C was used with olivine as an oxygen carrier. After these reactions, the reactor turned completely black. One set of results of these preliminary experiments and a picture of the blackened reactor is shown in appendix 11.4. The SEM pictures of sample 5 are not shown, since the deposition found on the reactor walls was non-conductive. It most likely will only be carbon.

** After the ilmenite reactions, when the reactor was cooled down and taken out, a difference in color between the top and bottom of the oxygen carrier in the packed bed could be seen. This is shown in figure X. These layers were separated and both analyzed with SEM.

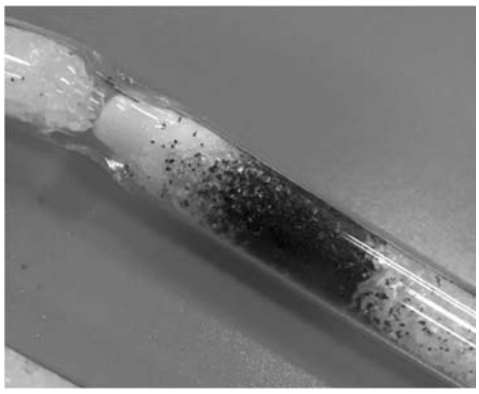

Fig. 29. Separate layers in the ilmenite packed bed after reaction.

a) Olivine SEM and EDX analysis

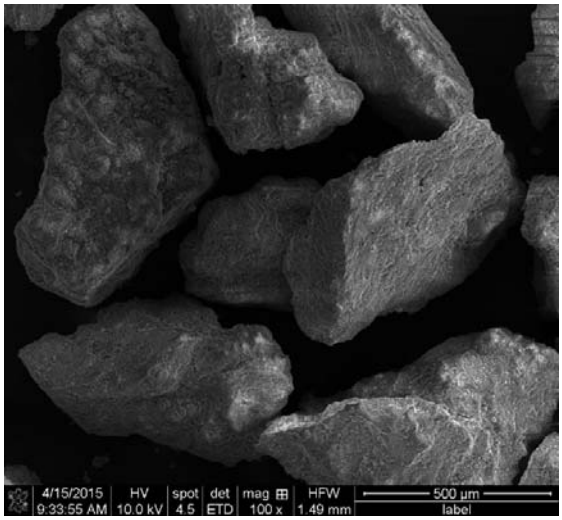

Fig. 30. Olivine sample 1, scale 500 µm.

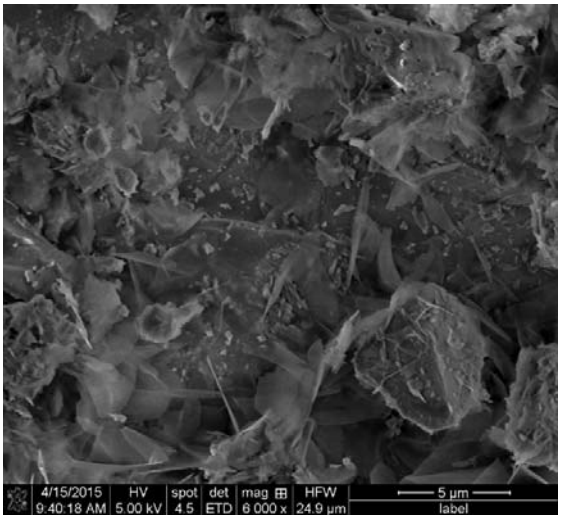

Fig. 31. Olivine sample 1, scale 5 µm.

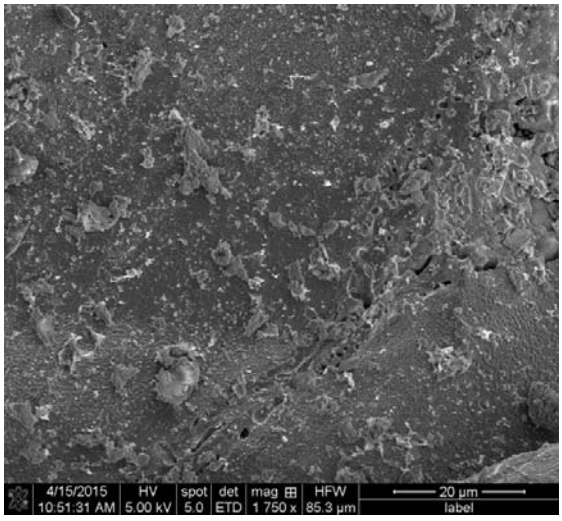

Fig. 32. Olivine sample 2, scale 20 µm.

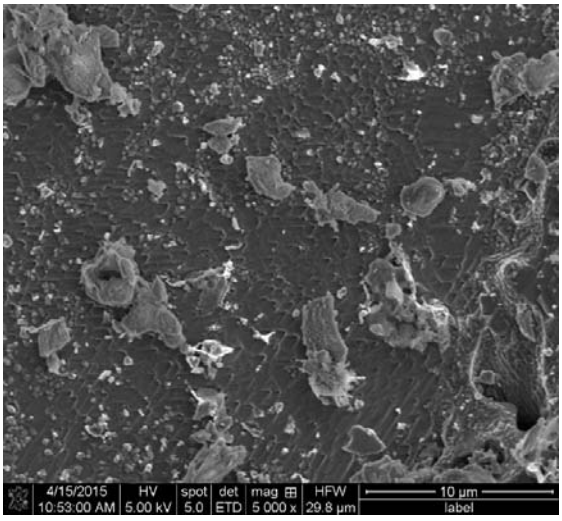

Fig. 33. Olivine sample 2, scale 10 µm.

The surface of the first olivine sample, the untreated olivine can be seen in figures 30 and 31. It was quite rugged. Thin, crystal-like structures could be seen at small scales. In table 17, on the next page, the surface composition in mass and atomic percentage determined by EDX is shown. The surface of untreated olivine consisted mostly of oxygen, magnesium, iron, silicon and calcium. Normally, there should only be a minimal amount of calcium in olivine from Magnolithe. The detected amount might be due to sample contamination. Besides that, EDX has only been measured on one spot in the sample.

After activation with air, the surface of the olivine changed which can be seen in figures 32 and 33. The surface seems smoother and a wave-like pattern could be seen. The composition of the surface has changed as well. The amount of silicon and magnesium at the surface has become much larger. The amount of iron has become twice as small, which does not conform with literature [32].

Table 17. EDX results of untreated olivine, sample 1.

Atom	Mass percentage (%)	Atomic percentage (%)
C	5.2	9.6
O	39	54
Mg	19	17
Al	0.90	0.74
Si	4.3	3.4
Ca	17	9.2
Fe	15	6.0

Table 18. EDX results of activated olivine, sample 2.

Atom	Mass percentage (%)	Atomic percentage (%)
O	40	54
Mg	33	29
Si	19	14
Fe	7.9	3.0

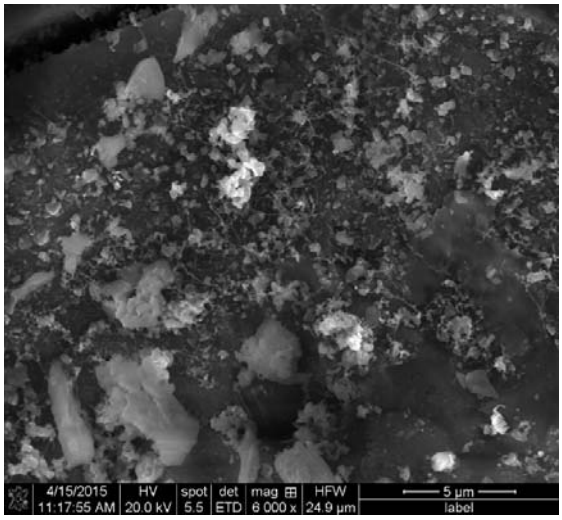

Fig. 34. Olivine sample 3, scale 5 µm.

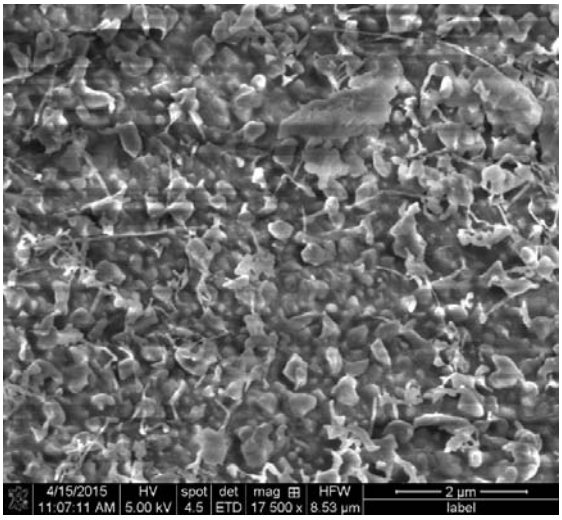

Fig. 35. Olivine sample 3, scale 2 µm.

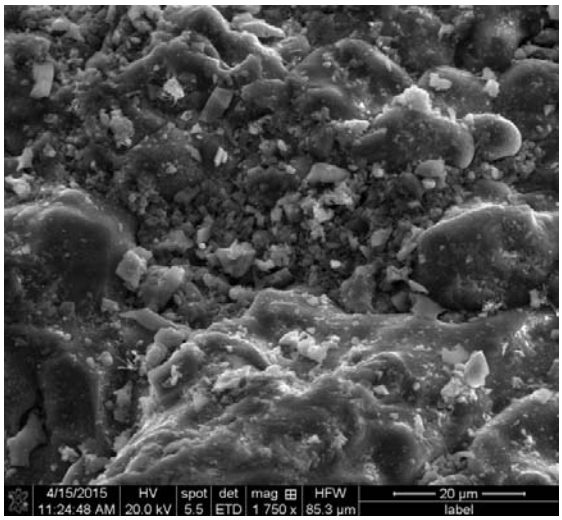

Fig. 36. Olivine sample 4, scale 20 µm.

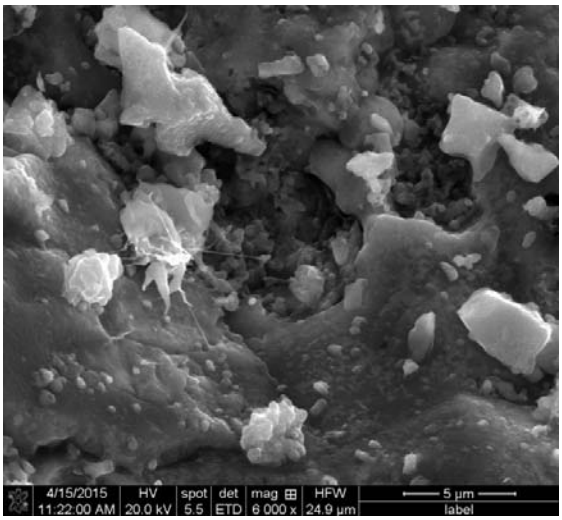

Fig. 37. Olivine sample 4, scale 5 µm.

The reaction with toluene, water and the gases at 800 ℃ caused a large change in the olivine surface. The surface was not smooth anymore and small particles appeared at the surface, some connected by wire-like structures seen in figures 34 and 35. This is observed in literature after treatment with air at 750 ℃ [29]. The amount of iron at the surface became larger, which can be seen in table 19, although nothing can be said about the phases in which the iron is present. There was some carbon present, most likely in the form of carbon deposition. The oxygen and magnesium at the surface decreased while the amount of silicon at the surface stays the same.

Table 19. EDX results of olivine after reaction at 800 ℃, sample 3.

Atom	Mass percentage (%)	Atomic percentage (%)
C	5.0	9.1
O	34	47
Mg	25	23
Si	18	14
Fe	17	6.8

Table 20. EDX results of olivine after reaction at 900 ℃, sample 4.

Atom	Mass percentage (%)	Atomic percentage (%)
C	20	30
O	40	44
Mg	23	17
Si	13	8.0
Fe	4.2	1.3

After reaction at 950 ℃, the structure was significantly different than after reaction at 800 ℃, which can be seen in figures 36 and 37. The surface appeared more porous and larger particles appeared at the surface. In comparison to reaction at 800 ℃, there was much more carbon at the surface, which can be seen in table 20. This explains the black appearance of the reactors after the reaction, discussed in the experimental section. The amount of oxygen at the surface was larger while the amount of magnesium, silicon and iron was lower.

To summarize, untreated olivine mostly had oxygen, magnesium and iron at the surface. Activation caused the surface to become more homogenous in appearance. After reaction, some carbon covered the surface and the amount of oxygen went down. When reaction was carried out at temperatures above 900 °C, much more carbon appeared at the surface and there was much less iron, magnesium and silicon. The iron enriched layer around olivine after oxidation, mentioned in the previous chapter [32], was not detected. This might be due to only a local measurement of EDX. It could be that the iron layer is formed more clearly after multiple cycles of oxidation and reduction.

b) Ilmenite SEM and EDX analysis

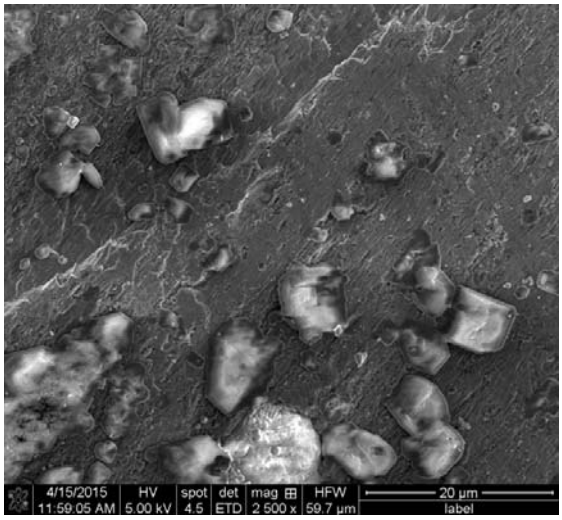

Fig. 38. Ilmenite sample 6, scale 20 µm.

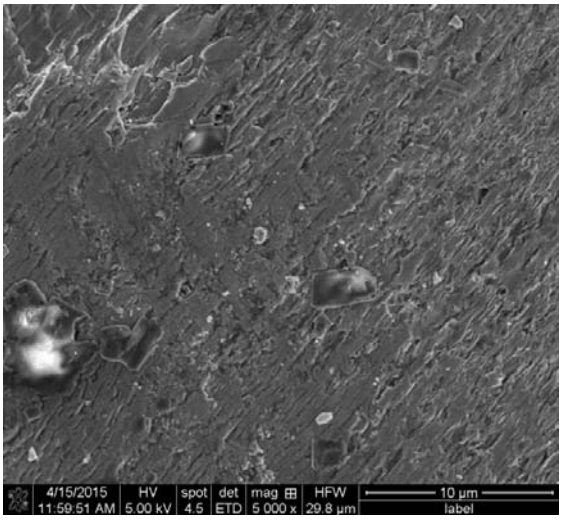

Fig. 39. Ilmenite sample 6, scale 10 µm.

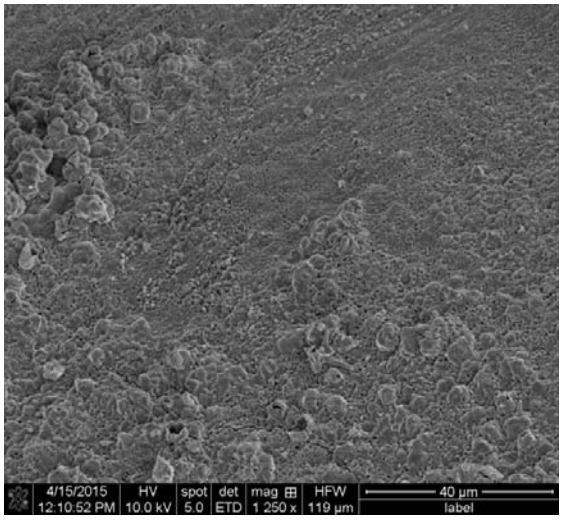

Fig. 40. Ilmenite, sample 7, scale 40 µm.

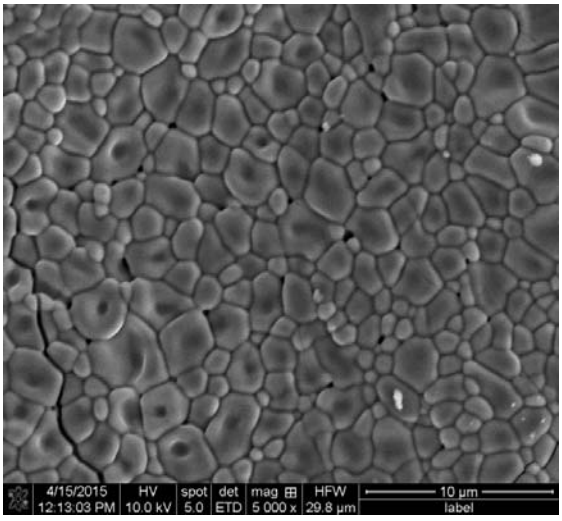

Fig. 41. Ilmenite, sample 7, scale 10 µm.

The surface of the untreated ilmenite, shown in figures 38 and 39, appeared quite smooth. It looked dense and no pores could be observed. The surface contained many different components, shown in table 21, but mostly consisted of oxygen, titanium and iron.

After activation with air, the surface changed severely. This can be seen in figures 40 and 41. A more porous structure could be seen with semi-spherical shapes. The amount of oxygen at the surface has become much larger. The amount of iron has almost doubled, shown in table 22, while the amount of titanium becomes smaller. This means iron migrates towards the surface, which is described in literature [33]. The large amount of carbon of the untreated ilmenite has completely vanished. This will most likely have been burned off by the reaction with air.

Table 21. EDX results of untreated ilmenite, sample 6.

Atom	Mass percentage (%)	Atomic percentage (%)
C	12	25
O	28	43
Mg	2.6	2.6
Al	0.57	0.52
Si	3.2	2.8
Ca	0.62	0.39
Ti	26	13
V	0.45	0.22
Mn	0.57	0.26
Fe	27	12

Table 22. EDX results of ilmenite after activation, sample 7.

Atom	Mass percentage (%)	Atomic percentage (%)
O	36	65
Mg	0.70	0.83
Si	0.58	0.59
Ti	14	8.4
V	0.23	0.13
Mn	0.76	0.40
Fe	48	25

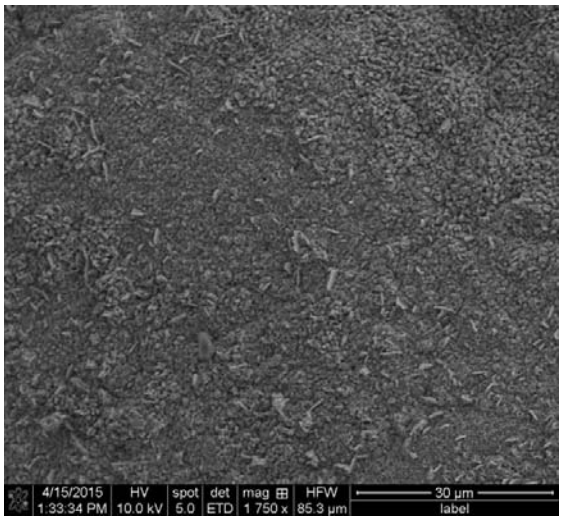

Fig. 42. Ilmenite, sample 8, scale 50 µm.

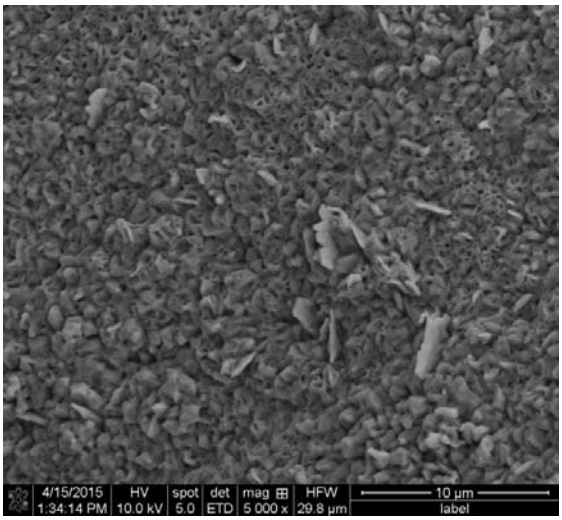

Fig. 43. Ilmenite, sample 8, scale 10 µm.

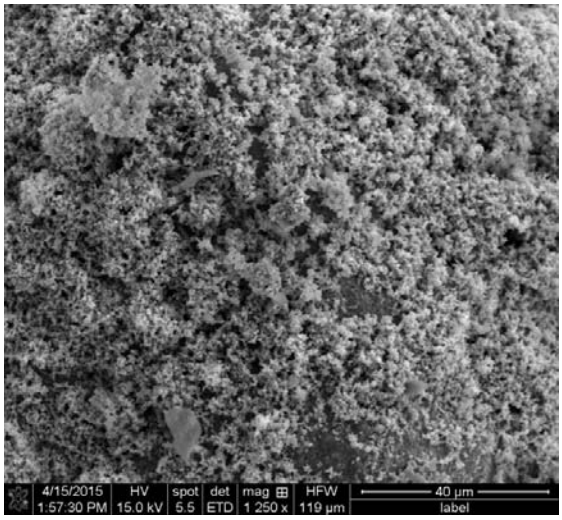

Fig. 44. Ilmenite, sample 9, scale 40 µm.

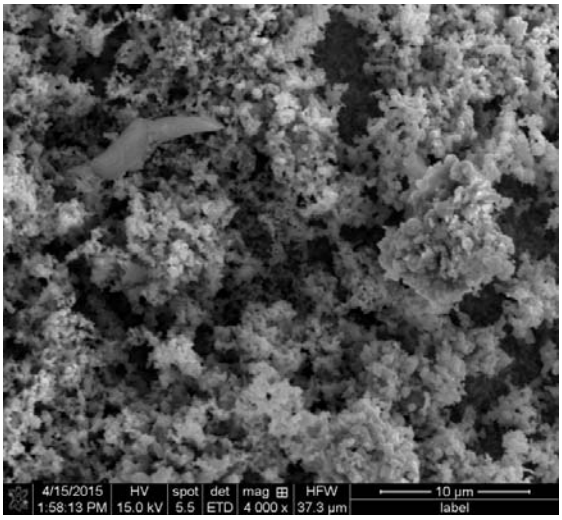

Fig. 45. Ilmenite, sample 9, scale 10 µm.

Table 23. EDX results of reacted ilmenite (bottom), sample 8.

Atom	Mass percentage (%)	Atomic percentage (%)
C	5.7	16
O	18	38
Mg	2.0	2.8
Sn	1.0	0.29
Ti	1.1	0.76
V	0.43	0.28
Mn	1.8	1.1
Fe	69	41

Table 24. EDX results of reacted ilmenite (top), sample 9.

Atom	Mass percentage (%)	Atomic percentage (%)
C	3.3	8.1
O	29	54
Mg	1.6	1.9
Al	1.0	1.1
Si	1.4	1.5
Ti	4.5	2.7
V	0.27	0.16
Fe	59	31

The bottom part of the oxygen carrier after reaction is shown in figure 42 and figure 43. The pores changed shape and became more edgy and sharp. The structure even appeared more porous than before reaction. There was much less oxygen and titanium at the surface than before while much more iron was present. This can be seen in table 23. This sample was taken from the bottom of the reacted ilmenite, so the part that was reached by the reaction gas last.

The top part of the oxygen carrier after reaction had a very different structure from the bottom part. The ilmenite particles became even more porous and a tree- or forest-like structure can be seen in figures 44 and 45. There was more oxygen at the surface then at the bottom part of the oxygen carrier and the amount of iron at the surface was smaller. More titanium reappeared at the surface, seen in table 24. Because of the change in color between the two parts of the reacted ilmenite, it might be that the iron present at the surface appeared in a different oxidation state and caused a change in color over time during reaction. The difference in oxidation state or the migration of metals and oxygen through the material could cause the difference in microstructure seen on the SEM pictures.

EDX has been measured at only one spot on the surface. To get a deeper understanding of the difference in structures, more spots should be sampled and multiple particles should be scanned. However, the purpose of these measurements was to get a general overview of the structural changes in the material, before and after activation and reaction.

In summary, ilmenite consisted of more different metals than olivine. Untreated ilmenite appears flat and dense and mostly had carbon, oxygen, titanium and iron at its surface. After activation, the structure of ilmenite became more porous and there was no carbon left. Iron migrated to the surface. After reaction, ilmenite had a different color at the top than at the bottom of the packed bed. The two differently colored parts were analyzed separately. For the bottom part of the material, the pores changed shape. They became more edgy and smaller. The top part of the reacted material had much deeper appearing pores and it had tree-like structures. The toluene steam reforming and gas reactions that were done made the oxygen content smaller and the iron content higher. Iron migration and different oxidation states of iron probably influence the color of the ilmenite. As mentioned in last chapter, it might take multiple oxidation and reduction cycles to get a stable, reduced form of ilmenite in the form Fe_2TiO_5 + TiO_2 [30], which will correspond to one surface structure of ilmenite. It would be recommended to obtain this stable form and analyze it with SEM and EDX.

6.7. Conclusion of the experimental analysis of oxygen carriers

The reactivity of olivine and ilmenite towards the reduction of toluene as a model tar component in the biomass gasification process were compared. Experiments in the kinetics set-up with water and toluene have been done. Ilmenite and olivine were both tested for their reactivity in several gas reactions. The structures of ilmenite and olivine on a micro scale have been analyzed by SEM and EDX.

Olivine converted toluene in the steam toluene reforming reaction to H_2, CO_2, CO and a very small amount of CH_4. This happened without the formation of many side products. Only traces of benzene were found when the liquid products of the reaction were analyzed by GC. The liquids condensed contained much more toluene than expected. Less water has condensed than predicted. The quantification of the liquid samples might not be reliable enough. Olivine was not very active in gas reactions that occur simultaneously in the gasifier. Only water-gas shift was catalyzed with a conversion of CO of about 8 %. The structure of olivine changed when the material was activated. Activation caused migration of iron. Reaction caused some carbon deposition to arise, but this was a small amount.

Ilmenite converted toluene into H_2, CO_2, CO and some CH_4 as well, but there were many side products formed at higher steam to toluene ratios. Traces of phenols and even toluene polymerization products were found when the liquid from the toluene steam reforming reactions were analyzed by GC-MS. SEM pointed out that in ilmenite, quite dramatic structural changes occurred. The untreated material appeared flat, activation made the structure more porous and reaction gravely changed the shape of those pores.

Olivine and ilmenite both seem to have similar activity towards toluene as a model tar component. From the experiments, olivine seems a better choice for toluene steam reforming because of the lack of side products. Especially polymerization of tars must be avoided. Phenol formation is unwanted, especially because phenol is poisonous, but tar formed in biomass gasification might already contain phenols or other carcinogenic components. The structure of both oxygen carriers changed with activation and reaction. More oxidation and reduction cycles are necessary to determine if a stable structure is reached for both olivine and ilmenite and if this stable structure reacts differently than the material after normal air oxidation.

The activity experiments were compared to the data available in literature. According to Swierczynski et al. [3], the given toluene steam reforming reactions are a simplification. Methane formed in side reactions is not mentioned. A comparison of olivine and olivine doped with nickel at different temperatures from [3] is shown. It shows that at 850 °C, Ni-olivine has a conversion which is about three times larger than the conversion of pure olivine. When the kinetic data of olivine doped with nickel were applied to a plug flow reactor of the same size as the experimental set-up, a conversion of 30 % of the toluene at the inlet was predicted. The estimation is shown in appendix 11.8. In the olivine activity experiments, the conversion was less than 1 %. The k value of the olivine from experiments is estimated to be around 10^3 times smaller than the k value of olivine with nickel. To get more insight into the differences between olivine and Ni-olivine, the activation energy must be determined. Hence, a complete kinetics study must be done.

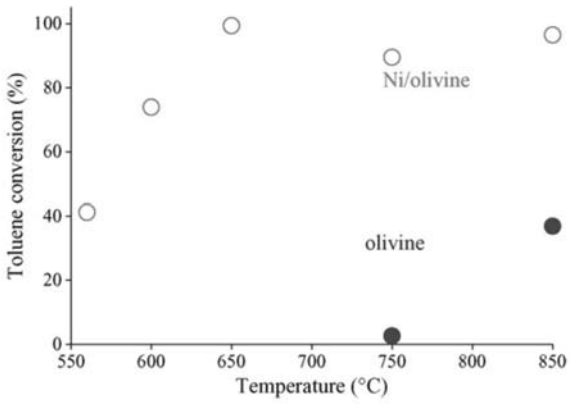

Fig. 46. Comparison of olivine and olivine doped with nickel from Swiercynski et al. [3]

7. Phenomenological model

To test the use of the oxygen carriers in an indirect biomass gasifier, the whole system is modeled in Aspen Plus. Aspen Plus is a process simulator in which complete production processes can be modeled. The model for biomass gasification will be used for the prediction of tar conversion in various circumstances. The goal is to achieve as much syngas production as possible. A preliminary TNEE model with sand as the circulating bed material was already in place [2]. This model is expanded and improved to give a more realistic view on the conversion of tar in the system. The different tars are reduced to only one model tar component, which is toluene, and the kinetic tar reduction reactions with the oxygen carriers were incorporated. Ilmenite was incorporated in the model before but the results were not comparable to data in open literature, mainly because of the assumption that toluene was partially oxidized. In the present work, toluene steam reforming was chosen as a model reaction for a better understanding of tar destruction. The model was further expanded to include reduction and oxidation of the oxygen carriers. These reactions were modeled separately from their kinetic tar reduction capabilities to ensure a result comparable to literature and experiments.

7.1. TNEE model with sand as bed material

The TNEE model with sand was modeled in a previous graduation project [2]. It was done according to Abdelouahed et al. [1]. The Tunzini Nessi Equipment Companies (TNEE) process is used, of which details can be found in section 2.5. The process consists of two low-velocity fluidized beds (LVFB). The first fluidized bed, the gasifier, is split into three parts in Aspen plus. It is split into the pyrolysis, the dense zone (fluidization zone), and the secondary reaction zone (freeboard). The pyrolysis is not a real zone. It represents the pyrolysis of biomass that happens instantaneously. A schematic representation of the gasifier divided in three parts is given in figure X. Sand is used as a bed material for this model, it supplies heat to the gasifier and is heated up in the combustor. The sand facilitates char gasification in the dense zone of the gasifier. The amount of char produced is based on the remaining carbon and hydrogen from the biomass pyrolysis. The pyrolysis zone is modeled as a yield reactor (PYROL) where the biomass and sand are fed together. The pyrolysis temperature is 760 °C. The yields of the gaseous compounds are calculated with the correlations from literature [1]. Char production is calculated with the carbon elemental balance. The mass balance is then closed by recalculating the yield of water [44]. The elemental composition of the char is calculated from correlations by the same reference [44]. The heat duty for the pyrolysis is set to 0 to simulate the heat which is exchanged with the combustor. 14 % of the produced gas is recycled as fluidization gas. There is a bypass of fluidization gas around the pyrolysis. This is done because the yield reactor reacts to the overall mass flow and the yields would be wrong if the fluidization gas was included. Air is transported to the combustor. The required amount of air for the burning of all the char and tar in the combustor, is determined with a design specification. The mole fraction of oxygen in the flue gas is limited to 2 %.

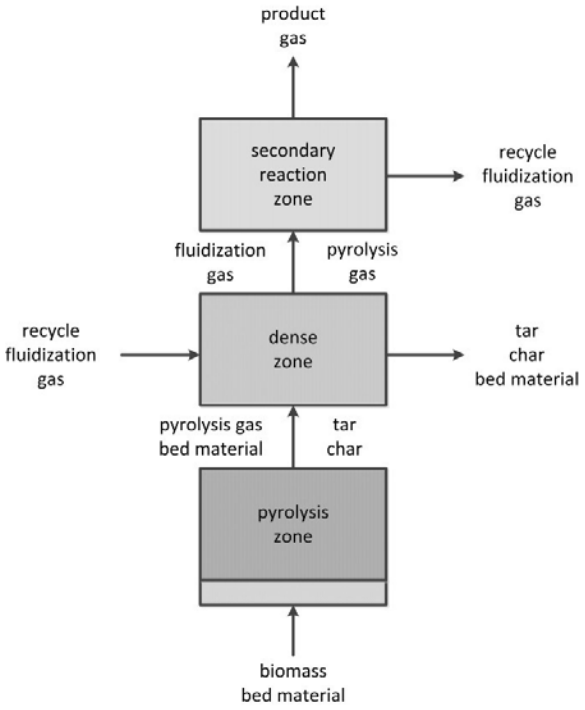

Fig. 47. Representation of the gasifier divided in three parts in Aspen Plus.

The following correlations are used for the product yield in pyrolysis (PYROL block) (table 25) and for the ultimate analysis for char decomposition in the DECOMP block, which is part of the combustor (table 26).

Table 25. Coefficients for pyrolysis product yield [2].

Product	a	b	c
CH_4	-4.341×10^{-5}	10.12×10^{-2}	-51.08
H_2	1.362×10^{-5}	-2.517×10^{-2}	12.19
CO	-3.524×10^{-5}	9.770×10^{-2}	-24.93
CO_2	3.958×10^{-5}	-9.126×10^{-2}	64.02
C_2H_4	-6.873×10^{-5}	14.94×10^{-2}	−76.89
C_2H_6	8.265×10^{-6}	-2.105×10^{-2}	13.38
C_6H_6	-3.134×10^{-5}	7.544×10^{-2}	-42.72
C_7H_8	-4.539×10^{-6}	0.687×10^{-2}	1.462
C_6H_6O	1.508×10^{-5}	-3.662×10^{-2}	22.19
$C_{10}H_8$	-8.548×10^{-6}	1.882×10^{-2}	-9.851
H_2O	5.157×10^{-5}	11.86×10^{-2}	84.91

Table 26. Correlations for the char ultimate analysis calculation. $aT^2 + bT + c$ [2].

Element	a	b	c
C	-2.4977×10^{-7}	6.60002×10^{-4}	-0.507874935
H	1.6601×10^{-7}	-4.0765×10^{-4}	0.260630036
O	1-(C+H)		

The reactions used in the Aspen Plus model are summarized in table 27. They include char and soot gasification and the water-gas shift reaction.

Table 27. Reactions used in the TNEE model in Aspen plus.

Nr.	Reaction name	Reaction	Reaction rate (kmol/m³s)
1	Char gasification [45]	$C_xH_yO_z + (x - y)H_2O \rightarrow xCO + \left(x - z + \frac{y}{2}\right)H_2$	$R = 4.8 \cdot 10^4 \cdot \exp\left(\frac{-211000}{RT}\right)\rho_{H_2O}^{0.51}$
2	Soot gasification [46]	$C + H_2O \rightarrow CO + H_2$	$R = 3 \cdot 10^{11} \cdot \exp\left(\frac{-310000}{RT}\right)\frac{m_{soot}}{V_R}C_{H_2O}$
3	Water gas shift [47]	$CO + H_2O \rightarrow CO_2 + H_2$	$R = 5.2 \cdot 10^{11} \cdot \exp\left(\frac{-102400}{RT}\right)C_{H_2O}C_{CO}$
4	Reverse WGS [48]	$CO_2 + H_2 \rightarrow CO + H_2O$	$R = 5.2 \cdot 10^{10} \cdot \exp\left(\frac{-31300}{RT}\right)C_{H_2}^{0.5}C_{CO_2}$
5	Carbon combustion (combustor) [1]	$C + O_2 \rightarrow CO_2$	$X_C = 100\%$
6	Hydrogen combustion (combustor) [1]	$H_2 + \frac{1}{2}O_2 \rightarrow H_2O$	$X_{H_2} = 95\%$

7.2. Expansion and improvement of the TNEE model with sand

Figure 48 displays the flowsheet built up in Aspen Plus. The circulation bed material in the model is sand. The flowsheet has four blocks which have Fortran routines. Fortran routines are user defined models to extend the modelling capabilities of Aspen Plus. The routines are added to the pyrolysis with the correlations described in table 25, the dense zone, the secondary reaction zone and the char decomposition with the correlations of table 26, which is a part of the combustor. The routines are simplified and enhanced so the model runs faster and with less errors and warnings.

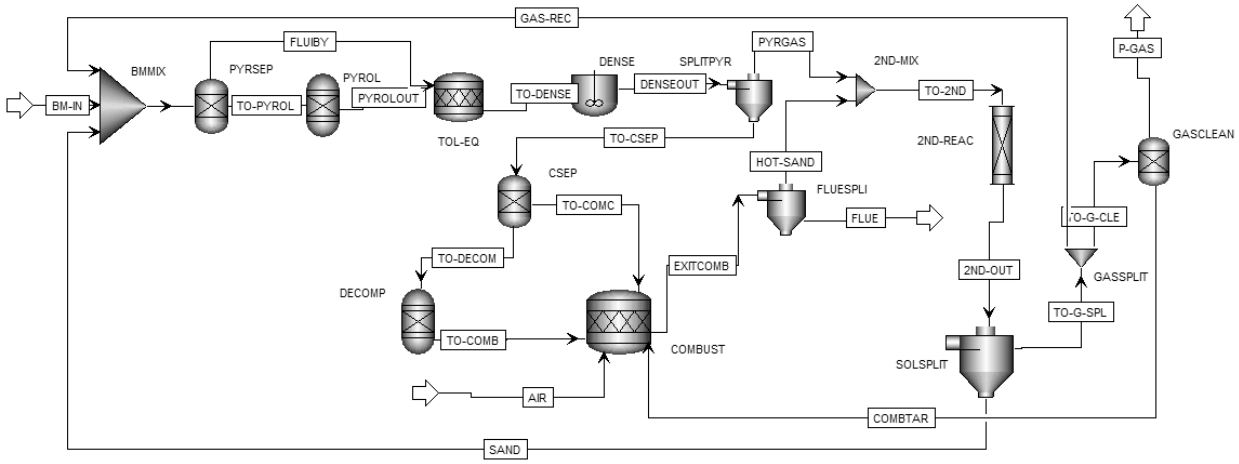

Fig. 48. TNEE model of biomass gasification in Aspen Plus.

In pyrolysis, ethylene (C_2H_4), ethane (C_2H_6), benzene (C_6H_6), toluene (C_6H_7), carbolic acid (C_6H_6O) and naphthalene ($C_{10}H_8$) are formed. After the pyrolysis block, an extra stoichiometric reactor called TOL-EQ is placed to lump the different components with higher carbon contents into only one model tar component, which is toluene. The results of the simulations with the improved flowsheet are given in table 28. As mentioned before, the fluidization gas bypasses the pyrolysis.

Table 28. Results of pyrolysis and tar lumping in the Aspen Plus flowsheet with sand.

Flow	Unit	TO-PYROL	FLUIBY	PYROLOUT	TO-DENSE	DENSEOUT	TO-2ND	P-GAS
Biomass	kg/hr	4970	0	0	0	0	0	0
Char	kg/hr	0	0	480	480	476	23.8	0
CH_4	kmol/hr	0	2.41	14.8	17.2	17.2	17.2	14.8
H_2	kmol/hr	0	4.72	15.2	23.5	24.3	24.3	29.0
CO	kmol/hr	0	6.25	44.0	50.2	50.1	50.1	38.4
CO_2	kmol/hr	0	2.61	8.05	10.7	11.1	11.1	16.0
C_2H_4	kmol/hr	0	0	4.73	0	0	0	0
C_2H_6	kmol/hr	0	0	0.222	0	0	0	0
C_6H_6	kmol/hr	0	0	0.947	0	0	0	0
C_7H_6	kmol/hr	0	0.448	0.199	3.20	3.20	3.20	0
C_6H_6O	kmol/hr	0	0	0.0455	0	0	0	0
$C_{10}H_8$	kmol/hr	0	0	0.200	0	0	0	0
H_2O	kmol/hr	0	19.8	132	151	151	151	122

The TOL-EQ block stoichiometrically lumps the tars formed in the pyrolysis to toluene. The lumped toluene is underlined in table 28. Part of the tar is recycled with part of the produced gas as fluidization gas (14 %). The other part is burned in the combustor together with the char. A small amount (about 6 mass percent) of char is reformed with water in the dense zone and the secondary reaction zone. 319 kmol/hr of air is added to the combustor to burn the char and tar produced. 221 kmol/hr of product gas is produced. The molar fraction of syngas in the product gas is 20 %, the amounts in kmol/hr are underlined in the table. The results of the produced gases at the outlet are the same as the results that were achieved in a prior graduation project [2].

7.3. Addition of catalytic bed material

There were no kinetics found in open literature for a toluene reduction reaction with olivine. The only kinetics found are for the toluene steam reforming in the presence of nickel doped olivine [23]. The kinetic expression is shown in table 29. The reaction rate is valid for the first order toluene decomposition. The two reactions given are a simplification of the reactions that occur for toluene steam cracking at high temperatures. It is assumed that water gas shift occurs simultaneously, which can be seen in the second reaction. These kinetics are used for both olivine and ilmenite, as the main tar steam reforming mechanism mentioned in section 5.5 is catalyzed by the iron present in the material. From the experimental section, it was already pointed out that olivine without nickel is much less active. Nevertheless, the kinetics with nickel are still used as more data of a detailed kinetics study is necessary for the pure olivine. The reactions provided occur in the gasifier, in the dense zone. No catalytic material is added to the flowsheet, only the kinetics for the reforming reaction. The kinetics are based on a dense zone of 8 m^2, a porosity of 0.47 and a density of the catalytic material of 3320 kg/m^3.

From activity experiments, it was estimated that the k value of olivine without nickel is around 10^3 times smaller than the k value of olivine doped with nickel. If only the k value is changed in the Aspen Plus flowsheet, the results do not change. In order to see the difference between olivine and Ni-olivine, the activation energy of the reactions with olivine need to be determined.

Table 29. Kinetics of toluene steam reforming reactions in the presence of Ni-doped olivine.

Nr.	Reaction name	Reaction	Reaction rate (kmol/m^3s)
1	Toluene steam reforming [23]	$C_7H_8 + 7\,H_2O \rightarrow 7\,CO + 11\,H_2$	$R = 8.72 \cdot 10^9 \cdot \exp\left(\frac{-196000}{RT}\right) \frac{m_{solid}}{V} C_{C_7H_8}$
2		$C_7H_8 + 14\,H_2O \rightarrow 7\,CO_2 + 18\,H_2$	

The reaction rate is valid for the first order toluene decomposition [23]. The two reactions given are a simplification of the reactions that occur for toluene steam cracking at high temperatures. It is assumed that water gas shift occurs simultaneously, which can be seen in the second reaction.

The most important side reactions that have to be taken into account are carbon deposition reactions by decomposition of C_7H_8 or CH_4 and by CO disproportionation, which is the Boudouard reaction. Carbon deposition occurs if the gas does not contain enough oxidizing component (H_2O) or if the reaction temperature is below 650 °C, as the main carbon formation reaction (2 CO $\rightleftarrows$ CO + C) is favorable at temperatures lower than 650 °C. The steam reforming reactions become thermodynamically favorable at temperatures higher than 435 °C and 350 °C, respectively. The most favorable conditions for carrying out the toluene reforming reaction are above 650 °C. The gasifier temperature of 760 °C in the TNEE model assures that this side reaction can be ignored.

Table 30. Results of pyrolysis and tar lumping in the Aspen Plus flowsheet with sand.

Flow	Unit	TO-DENSE	DENSEOUT	TO-2ND	P-GAS
Biomass	kg/hr	0	0	0	0
Char	kg/hr	481	479	23.9	0
CH_4	kmol/hr	17.2	17.2	17.2	14.8
H_2	kmol/hr	27.2	51.8	51.8	52.8
CO	kmol/hr	52.7	67.8	67.8	53.9
CO_2	kmol/hr	10.6	11.0	11.0	15.8
C_2H_4	kmol/hr	0	0	0	0
C_2H_6	kmol/hr	0	0	0	0
C_6H_6	kmol/hr	0	0	0	0
C_7H_6	kmol/hr	2.85	0.661	0.661	0
C_6H_6O	kmol/hr	0	0	0	0
$C_{10}H_8$	kmol/hr	0	0	0	0
H_2O	kmol/hr	149	133	133	106

For the simulation, the amount of biomass at the inlet is kept constant. As can be seen in table 30, the amount of tar produced in the gasifier has greatly reduced. Similar to the data in literature [3], 77 % of the combined tar produced in the pyrolysis has been reformed. A much smaller amount of tar needed to be burned in the combustor. As a consequence, only 213 kmol/hr of air was needed to for the burning in the combustor. The amount of syngas in the product gas has risen to 244 kmol/hr. The molar fraction of syngas in the product gas was 43 %. Steam tar reforming in the presence of catalytic bed material has more than doubled the amount of syngas produced.

7.4. Addition of oxidation and reduction reaction

To represent the oxygen carriers in a more realistic way, oxidation and reduction reactions for iron hydroxides [34] [49] are added to the Aspen Plus flow sheet, shown in table 31. They occur in the dense zone of the gasifier. The oxidation reaction ($4\,FeO + O_2 \rightarrow 2\,Fe_2O_3$) is not added as a kinetic reaction but as a complete conversion reaction in the combustor.

Table 31. Kinetics of iron hydroxide reduction reactions.

Nr.	Reaction name	Reaction	Reaction rate (kmol/m^{3}s)
1	Iron hydroxide reduction reactions [34][49]	$Fe_2O_3 + H_2 \rightarrow 2\,FeO + H_2O$	$R = 2.15 \cdot 10^1 \cdot \exp\left(\frac{-65000}{RT}\right) C_{H_2}$
2		$Fe_2O_3 + CO \rightarrow 2\,FeO + CO_2$	$R = 3.46 \cdot 10^1 \exp\left(\frac{-80700}{RT}\right) C_{CO}$
3		$4\,Fe_2O_3 + CH_4 \rightarrow 8\,FeO + CO_2 + 2\,H_2O$	$R = 3.39 \cdot 10^3 \cdot \exp\left(\frac{-132200}{RT}\right) C_{CH_4}$

The iron hydroxides were added to Aspen Plus as a vapor. This is done because in Aspen Plus, it is not possible to model gas-solid reactions. As a consequence, all cyclones were changed to separators to split both the sand and the iron hydroxides from the gases. To add the kinetic reactions to the flowsheet, a separate CSTR was added after the dense zone in which the tar steam reforming reactions occur. This is done so the second CSTR could have different dimensions from the first one. If the kinetics of the iron hydroxide reduction reactions were added to the first CSTR, the kinetics were incorrectly implemented by Aspen Plus. This lead to the decision to make the dimensions of the second CSTR much smaller. Its size was determined to get a realistic amount of iron hydroxides in the system, similar to the amount used in the simulations done in a prior graduation project [2]. The volume of the second dense zone used, was 0.4 m^3.

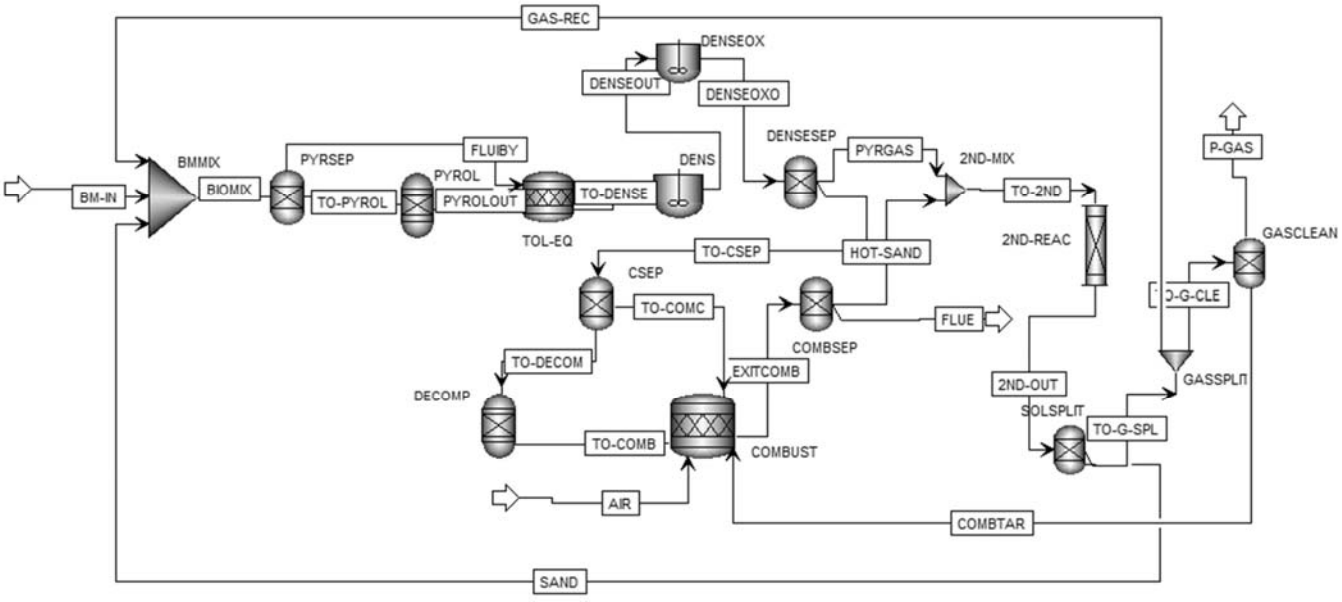

Fig. 49. Aspen flowsheet including iron hydroxide kinetics.

The amount of iron hydroxide used was varied. It depends on which oxygen carrier is used and what mass fraction of that oxygen carrier is used.

The amount of biomass at the inlet was kept the same as the simulations before. The inert part of olivine and ilmenite is modeled equal to sand. The TO-PYROL and FLUIBY and PYROLOUT streams are not shown anymore. In the table below, the results of experiments with 10 wt% olivine are shown in table 32. The other tar components are zero in these streams.

Table 32. Results of simulations with the Aspen Plus flowsheet with 10 wt% olivine.

Flow	Unit	TO-DENSE	DENSEOUT	DENSEOXO	TO-2ND	P-GAS
Char	kg/hr	517	515	515	515	0
CH_4	kmol/hr	17.4	17.4	17.3	17.3	14.9
H_2	kmol/hr	29.9	53.5	51.8	51.8	75.9
CO	kmol/hr	58.3	72.8	72.4	72.4	81.1
CO_2	kmol/hr	11.1	11.4	11.9	11.9	15.7
C_7H_6	kmol/hr	2.88	0.778	0.778	0.778	0
H_2O	kmol/hr	153	138	140	140	91.6

The oxygen necessary in the combustor was 34.7 kmol/hr. Because of the presence of the activated oxygen carriers, less air needs to be added to the combustor. The molar fraction of syngas in the product gas was 54 %, which is larger than without implementation of the oxygen carrier. The conversion of the tar in the dense zone was 73 %, which is a little less than without the oxygen carrier. 14 % of the tar and product gases is recycled to the inlet of the gasifier. As the amount of product gases becomes larger, the fraction of tar recycled is smaller which causes this slight change in tar conversion.

Results of experiments with 10 wt% ilmenite are shown in table 33. The other tar components are zero in these streams.

Table 33. Results of simulations with the Aspen Plus flowsheet with 10 wt% ilmenite.

Flow	Unit	TO-DENSE	DENSEOUT	DENSEOXO	TO-2ND	P-GAS
Char	kg/hr	522	520	520	520	0
CH_4	kmol/hr	17.4	17.4	16.9	16.9	14.6
H_2	kmol/hr	27.8	50.8	38.7	38.7	64.0
CO	kmol/hr	58.0	72.2	69.2	69.2	78.3
CO_2	kmol/hr	11.5	11.8	15.3	15.3	18.1
C_7H_6	kmol/hr	2.89	0.829	0.829	0.829	0
H_2O	kmol/hr	156	141	154	154	105

In comparison to the case with 10 wt% of olivine, there is more active bed material in 10 wt% ilmenite due to its higher iron content. As a consequence, more H_2, CO and CH_4 is used in the reduction reactions which results in an overall lower amount of syngas (46 %) in the product gas. It would be expected that more active material would result in more tar steam reforming and therefore more gas production, but the small changes in k-value in the Arrhenius equation are not enough to reduce the tar more. A conversion of 71 % is achieved. 43.3 kmol/hr of air is needed in the combustor, this is again due to the larger amount of iron that needs to be oxidized after a cycle.

The amount of syngas produced was investigated at different oxygen carrier levels. The results for ilmenite and olivine are shown in figure 50 and 51 respectively.

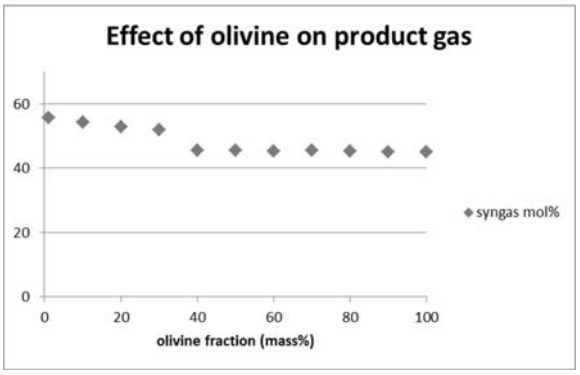

Fig. 50. Effect of olivine on syngas production.

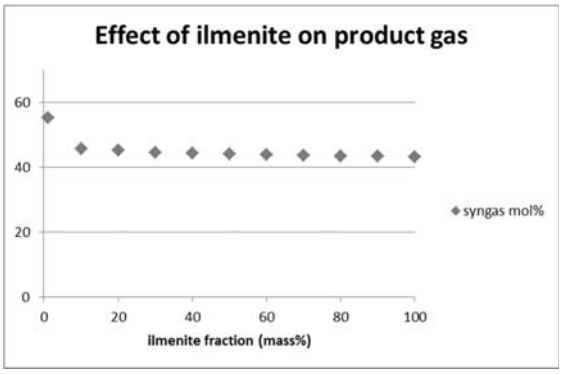

Fig. 51. Effect of ilmenite on syngas production.

The tar conversion for olivine decreased when more oxygen carrier is added, but only slightly. The produced amount of syngas stayed more or less constant until 40 wt% of olivine. At 40 wt% there was a decrease in the amount of syngas produced. The higher iron content of ilmenite has a negative effect on the produced gases due to the reduction reactions, the more sharp decrease in syngas production for ilmenite already occurs at 10 wt%.

To summarize, a model was set up for the use of catalysts in biomass gasification. All different tar components were lumped to only toluene as a model tar component. Toluene reduction reactions for nickel-doped olivine were added. These reactions reduced the overall toluene content, comparable to values achieved in literature [23]. Then, oxidation and reduction reactions of iron hydroxides in the oxygen carriers were added. This gives a more realistic result regarding the produced gases. However, the iron oxide is modeled in the vapor phase, because gas-solid kinetic reactions cannot be modeled in Aspen Plus. The flow sheet can be used for different oxygen carriers as long as detailed kinetic data is available. In table 34, the results of the different models can be seen.

Table 34. Comparison of results of the simulations in the Aspen Plus models.

Model	Tar reduction (%)	Product gas (kmol/hr)	Syngas in product gas (%)	Air needed for tar and char burning (kmol/hr)
Sand	0	221	20	319
Tar reduction kinetics	77	244	43	213
Tar reduction and iron hydroxides kinetics *	73	279	54	34.7

* These are the results for 10 wt% olivine as active bed material, the rest of the bed material is sand.

8. Conclusions and recommendations

The main goal of this project was the development of a phenomenological model for indirect biomass gasification using an oxygen carrier as bed material for the optimal production of syngas. This was achieved by setting up a model in Aspen Plus that can support the catalytic activity of oxygen carriers and their reduction and oxidation reactions. Olivine and ilmenite were used as oxygen carriers. The activity of olivine and ilmenite were compared in gas and tar reforming experiments with toluene as a model tar component. A model was designed for the use of catalytically active oxygen carriers in biomass gasification, using the knowledge gained in experimental work.

The natural occurring minerals olivine and ilmenite offer some potential as cheap and environmentally friendly oxygen carriers [50] that can be used for tar reduction in biomass gasification. Ilmenite has a larger iron content than olivine which leads to faster oxidation and reduction of the oxygen carrier. Olivine can transport 0.5 wt% of oxygen [32] while ilmenite can transport up to 4.0 wt% of oxygen [33]. Ilmenite and olivine both form an active layer of iron at the surface after consecutive oxidation and reduction cycles [32] [33]. The mechanism for catalytic decomposition of tars, proposed by Uddin et al. [37], suggests that the active species in tar reduction is iron oxide. As a consequence, the state of the iron at the surface area of the iron oxide catalyst thus plays a major role in the catalytic tar reduction. The mobility of the iron present in the oxygen carriers is a key factor as well.

Experiments were done to compare the activity of olivine and ilmenite in a packed bed reactor. The activity in tar reforming was investigated with experiments with water and toluene. Ilmenite and olivine were both tested for their reactivity in several gas reactions. All experiments were done at 800 ℃, as above that temperature, thermal cracking occurred. Olivine converted toluene in the steam toluene reforming reaction to H_2, CO_2, CO and a very small amount of CH_4. Only traces of side products were formed. Olivine was not very active in gas reactions that occur simultaneously in the gasifier.

The experiments with olivine were compared to kinetic data for toluene steam reforming in the presence of nickel doped olivine found in literature [3]. No kinetics were found for the toluene steam reforming reaction with olivine. According to [3], olivine without nickel is less active, which needs to be taken into account. For kinetic data with olivine, a detailed kinetic study needs to be done.

Ilmenite converted toluene into H_2, CO_2, CO and some CH_4 as well, but there were more side products formed at higher steam to carbon ratios. Traces of phenols and even toluene polymerization products were observed in the toluene steam reforming reactions. Tar polymerization must be avoided as larger tars can foul the reactor more easily. In the gas reactions, ilmenite was more active than olivine. Ilmenite clearly catalyzed the steam methane reforming reaction. For the water gas shift experiment, a reduction in activity over time could be seen. This will most likely be due to carbon deposition. Activation between the experiments might be necessary to investigate the cause of peaks at the start of experiments and the influence of carbon deposition. Olivine seems to be a better active bed material in biomass gasification as it has a similar activity to ilmenite, but it does not produce hazardous side products during tar reforming.

The structures of ilmenite and olivine on a micro scale have been analyzed by SEM and EDX. The structure of olivine changed when the material was activated. Activation caused migration of iron. Reaction caused a small amount of carbon deposition to arise. SEM pointed out that in ilmenite, quite dramatic structural changes occurred. The untreated material seemed flat, activation gave it a structure with rounded pores and reaction gravely changed the shape of those pores. Multiple oxidation and reduction cycles are necessary to determine if the structural changes in olivine and ilmenite influence the activity towards gases and tar reforming reactions. This could be done by TGA.

The TNEE model has been set up in a prior graduation project with sand as the bed material. This model is simplified and enhanced so the model runs faster and with less errors and warnings. The different tars that are formed in pyrolysis are lumped into one model tar component in a stoichiometric reactor. For this model, 221 kmol/hr of product gas was produced with a molar fraction of syngas of 20 %.

The model was expanded for tar reduction reactions with a catalyst. The kinetics with Ni-olivine were used as an estimation [3]. Olivine without nickel is much less active. The reactions provided occur in the gasifier, in the dense zone. No catalytic material was added to the flowsheet yet, only the kinetics for the reforming reaction. This resulted in a tar reduction in the dense zone of 77 %, which is comparable to results achieved in literature [3]. The gas production rose to 244 kmol/hr with a molar fraction of syngas of 43 %.

Finally, to represent the oxygen carriers in a more realistic way, oxidation and reduction reactions for iron hydroxides [34] [49] were added to the Aspen Plus flow sheet. They occur in the dense zone of the gasifier. The oxidation reaction of hydroxide was not added as a kinetic reaction but as a complete conversion reaction in the combustor. The iron hydroxides were added to Aspen Plus as a vapor. This is done because in Aspen Plus, it is not possible to model gas-solid reactions well. This caused some problems with the kinetics, which are suitable for gas-solid reactions. To bypass these issues, the iron hydroxide reactions were modeled in a separate, smaller CSTR reactor which functioned as the second part of the dense zone. Adding the oxidation and reduction reactions of iron hydroxide resulted in a gas production of 279 kmol/hr with a molar fraction of syngas of was 54 %, which is larger than without implementation of the oxygen carrier. The conversion of the tar in the dense zone was 73 %, which is a little less than without the oxygen carrier. The influence of the iron content of olivine and ilmenite was compared in simulations. This leads to the conclusion that for ilmenite, more product gas is used in reduction. This is due to its higher iron content. Overall, olivine showed a higher syngas production. The heat duty of the reactor could be investigated in Aspen Plus to determine if autothermal operation would be possible at certain reaction conditions.

It needs to be noted that the catalytic and oxygen carrier capabilities of olivine and ilmenite were modeled separately. As a consequence, the addition of more catalyst only had a small influence on the rate determined by the Arrhenius equation for tar destruction and a large influence on the amount of gas needed for the reduction of the oxygen carriers. This can be solved by modeling the kinetics in gas-solid reactions. However, this is not possible in Aspen Plus. To model the gas-solid reactions which occur in the gasifier, a different program needs to be used.

MATLAB can be used for a more realistic approach to the gas-solid reactions that occur in the dense zone. The Aspen Plus flow sheet has to communicate with the MATLAB dense zone to run the whole simulation. This can be done by connecting the two programs in several steps as it is not possible to connect MATLAB and Aspen Plus directly. It is possible to create a calculator block in Aspen Plus with a subroutine. This subroutine can export the input variables of Aspen Plus in Excel. The input variables can then be exported by Excel to a text file, which can be inserted in a MATLAB model. The output of the MATLAB model can be generated as a new text file, which can be loaded back to the original Excel file. The output of this Excel file is then linked back to the calculator block and the rest of the Aspen Plus flowsheet can be run. The programming scheme is shown in a diagram in figure 52. Some preliminary simulations using this programming scheme were successfully executed where a simple model of a batch reactor in MATLAB was written and linked to a simple batch reactor flow sheet in Aspen Plus. This programming scheme might be used for improvement of the gas-solid reactions in Aspen Plus.

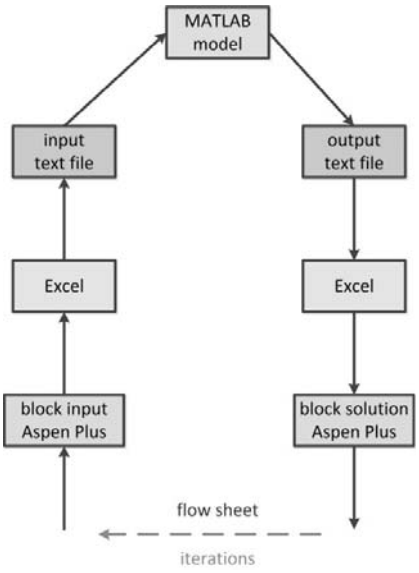

Fig. 52. Possible programming scheme for gas-solid reactions.

The main issues that would be recommended to be further investigated are:

- Multiple oxidation and reduction cycles should be done consecutively to determine if this influences the structural changes in olivine and ilmenite. This could be done by TGA. Furthermore, TGA could give more information about the activity towards gases and tar reforming reactions, now that more experimental data is available for experimental design.
- MATLAB can be used for a better representation of the dense zone in the gasifier or for the complete gasifier. The programming scheme described can be used to keep the rest of the flowsheet in Aspen Plus, or the complete system can be modeled in MATLAB. More detailed modeling of the gas-solid reactions will help gain more insight in the gas-solid reactions occurring.

9. Acknowledgement

I want to thank some people who helped me with this project. First prof.dr.ir. Martin van Sint Annaland for the fruitful discussions we had about the project. I want to thank dr. Fausto Gallucci as well, for helping me with the experimental work, the SEM and the interpretation of the results. I want to thank dr. Qi Wang for being my external committee member. I especially want to thank Ildefonso Campos Velarde for the support throughout the whole project. You coached me through the many difficulties we had in the lab and we even had some fun with the black reactors we made.

A special thanks to Joris Garenfeld for his help with troubleshooting in box 3. I want to thank Nerea Rodriguez Rodriguez MSc. for her help with the GC and ing. Wilko Weggemans for his help with the GC-MS. Furthermore, I would like to thank dr. Vincenzo Spallina for his help with the Aspen Plus Flowsheet. I really appreciate it.

I want to thank the whole SMR group for the time I had with you, I really enjoyed the atmosphere in the student room and the discussions we had over a cup of coffee (or tea). Bianca, thanks for TGIF and talking about our projects and the future, it really helped me to stay on track. Remco, thanks for proofreading my report and for your useful comments. Steven, thank you for your help with the report and keeping my stress levels below boiling point. I also want to thank my parents and my brother Nard for their support throughout the project.

10. Works cited

[1] L. Abdelouahed, O. Authier, and G. Mauviel, "Detailed modeling of biomass gasification in dual fluidized bed reactors under Aspen Plus," *Energy …*, 2012.

[2] V. R. A. Dhooge, "Fundamentals of chemical looping for biomass gasification," Eindhoven University of Technology, 2014.

[3] D. Swierczynski, C. Courson, and A. Kiennemann, "Study of steam reforming of toluene used as model compound of tar produced by biomass gasification," *Chem. Eng. Process. Process Intensif.*, vol. 47, no. 3, pp. 508–513, Mar. 2008.

[4] U.S. Department of Energy, "International Energy Outlook 2013," 2013. [Online]. Available: http://www.eia.gov/forecasts/ieo/world.cfm. [Accessed: 01-Jan-2014].

[5] UNFCC, "Status of Ratification of the Kyoto Protocol," 2005. [Online]. Available: http://unfccc.int/kyoto_protocol/status_of_ratification/items/2613.php. [Accessed: 01-Jan-2014].

[6] S. Rapagnâ, "Steam-gasification of biomass in a fluidised-bed of olivine particles," *Biomass and Bioenergy*, vol. 19, pp. 187–197, 2000.

[7] H. Schulz, "Short history and present trends of Fischer–Tropsch synthesis," *Appl. Catal. A Gen.*, vol. 186, pp. 3–12, 1999.

[8] C. van der Meijden, "Development of the MILENA gasification technology for the production of Bio-SNG," *Energy Res. Cent. Netherlands*, no. December, 2010.

[9] M. Ryden and a Lyngfelt, "Using steam reforming to produce hydrogen with carbon dioxide capture by chemical-looping combustion," *Int. J. Hydrogen Energy*, vol. 31, no. 10, pp. 1271–1283, Aug. 2006.

[10] R. E. Hester and R. M. Harrison, *Carbon capture: sequestration and storage*, 29th ed. Royal Society of Chemistry, 2009.

[11] W.-C. Yang, *Handbook of Fluidization and Fluid-Particle Systems*. New York: Chemical Industries, 2003.

[12] A. Gómez-Barea and B. Leckner, "Modeling of biomass gasification in fluidized bed," *Prog. Energy Combust. Sci.*, vol. 36, no. 4, pp. 444–509, Aug. 2010.

[13] J. Corella, J. M. Toledo, and M.-P. Aznar, "Improving the Modeling of the Kinetics of the Catalytic Tar Elimination in Biomass Gasification," *Ind. Eng. Chem. Res.*, vol. 41, no. 14, pp. 3351–3356, Jul. 2002.

[14] P. Morf, P. Hasler, and T. Nussbaumer, “Mechanisms and kinetics of homogeneous secondary reactions of tar from continuous pyrolysis of wood chips,” *Fuel*, vol. 81, no. 7, pp. 843–853, May 2002.

[15] L. P. L. M. Rabou, R. W. R. Zwart, B. J. Vreugdenhil, and L. Bos, “Tar in Biomass Producer Gas, the Energy research Centre of The Netherlands (ECN) Experience: An Enduring Challenge,” *Energy & Fuels*, vol. 23, no. 12, pp. 6189–6198, Dec. 2009.

[16] L. Devi, K. J. Ptasinski, F. J. J. G. Janssen, S. V. B. van Paasen, P. C. a. Bergman, and J. H. a. Kiel, “Catalytic decomposition of biomass tars: use of dolomite and untreated olivine,” *Renew. Energy*, vol. 30, no. 4, pp. 565–587, Apr. 2005.

[17] T. A. Milne and R. J. Evans, *Biomass Gasifier “ Tars ”: Their Nature , Formation , and Conversion Biomass Gasifier “ Tars ”: Their Nature , Formation , and Conversion*, no. November. 1998.

[18] J. Corella, M. Caballero, and M. Aznar, “A 6-lump model for the kinetics of the catalytic tar removal in biomass gasification,” *Proc. first world Conf. biomass energy Ind.*, pp. 1472–5, 2000.

[19] T. Mendiara, J. M. Johansen, R. Utrilla, P. Geraldo, A. D. Jensen, and P. Glarborg, “Evaluation of different oxygen carriers for biomass tar reforming (I): Carbon deposition in experiments with toluene,” *Fuel*, vol. 90, no. 3, pp. 1049–1060, Mar. 2011.

[20] J. Corella, J. M. Toledo, and R. Padilla, “Olivine or dolomite as in-bed additive in biomass gasification with air in a fluidized bed: Which is better?,” *Energy and Fuels*, vol. 18, no. 120, pp. 713–720, 2004.

[21] J. Delgado, M. P. Aznar, and J. Corella, “Biomass gasification with steam in fluidized bed: effectiveness of CaO, MgO, and CaO-MgO for hot raw gas cleaning,” *Industrial & Engineering Chemistry Research*, vol. 36, no. 5. pp. 1535–1543, 1997.

[22] R. J. Lancee, “Characterization and Reactivity of Olivine and Model Catalysts for Biomass Gasification,” Eindhoven University of Technology, 2014.

[23] D. Świerczyński, S. Libs, C. Courson, and a. Kiennemann, “Steam reforming of tar from a biomass gasification process over Ni/olivine catalyst using toluene as a model compound,” *Appl. Catal. B Environ.*, vol. 74, no. 3–4, pp. 211–222, Jul. 2007.

[24] Z. Min, M. Asadullah, P. Yimsiri, S. Zhang, H. Wu, and C. Z. Li, “Catalytic reforming of tar during gasification. Part I. Steam reforming of biomass tar using ilmenite as a catalyst,” *Fuel*, vol. 90, no. 5, pp. 1847–1854, 2011.

[25] C. Klein and C. S. Hurlburt, *Manual of Mineralogy*. New York: John Wiley & Sons, 1985.

[26] J. N. Kuhn, Z. Zhao, L. G. Felix, R. B. Slimane, C. W. Choi, and U. S. Ozkan, “Olivine catalysts for methane- and tar-steam reforming,” *Appl. Catal. B Environ.*, vol. 81, no. 1–2, pp. 14–26, 2008.

[27] H. Sibum, V. Güther, O. Roidl, F. Habashi, and H. U. Wolf, “Titanium, titanium alloys, and titanium compounds,” *… Ind. Chem.*, vol. 37, no. 55, 2000.

[28] M. Virginie, C. Courson, D. Niznansky, N. Chaoui, and A. Kiennemann, “Characterization and reactivity in toluene reforming of a Fe/olivine catalyst designed for gas cleanup in biomass gasification,” *Appl. Catal. B Environ.*, vol. 101, no. 1–2, pp. 90–100, 2010.

[29] H. O. a Fredriksson, R. J. Lancee, P. C. Thüne, H. J. Veringa, and J. W. H. Niemantsverdriet, “Olivine as tar removal catalyst in biomass gasification: Catalyst dynamics under model conditions,” *Appl. Catal. B Environ.*, vol. 130–131, pp. 168–177, 2013.

[30] J. Adánez, A. Cuadrat, A. Abad, P. Gayán, L. F. De Diego, and F. García-Labiano, “Ilmenite activation during consecutive redox cycles in chemical-looping combustion,” *Energy and Fuels*, vol. 24, no. 2, pp. 1402–1413, 2010.

[31] a. Fossdal, E. Bakken, B. a. Øye, C. Schøning, I. Kaus, T. Mokkelbost, and Y. Larring, “Study of inexpensive oxygen carriers for chemical looping combustion,” *Int. J. Greenh. Gas Control*, vol. 5, no. 3, pp. 483–488, 2011.

[32] R. J. Lancee, a. I. Dugulan, P. C. Thüne, H. J. Veringa, J. W. Niemantsverdriet, and H. O. a. Fredriksson, “Chemical looping capabilities of olivine, used as a catalyst in indirect biomass gasification,” *Appl. Catal. B Environ.*, vol. 145, pp. 216–222, Feb. 2014.

[33] a. Cuadrat, a. Abad, J. Adánez, L. F. De Diego, F. García-Labiano, and P. Gayán, “Behavior of ilmenite as oxygen carrier in chemical-looping combustion,” *Fuel Process. Technol.*, vol. 94, no. 1, pp. 101–112, 2012.

[34] A. Abad, J. Adánez, A. Cuadrat, F. García-Labiano, P. Gayán, and L. F. de Diego, “Kinetics of redox reactions of ilmenite for chemical-looping combustion,” *Chem. Eng. Sci.*, vol. 66, no. 4, pp. 689–702, 2011.

[35] H. Leion, A. Lyngfelt, M. Johansson, E. Jerndal, and T. Mattisson, “The use of ilmenite as an oxygen carrier in chemical-looping combustion,” *Chem. Eng. Res. Des.*, vol. 86, no. 9, pp. 1017–1026, Sep. 2008.

[36] X. Nitsch, J. M. Commandré, P. Clavel, E. Martin, J. Valette, and G. Volle, “Conversion of phenol-based tars over olivine and sand in a biomass gasification atmosphere,” *Energy and Fuels*, vol. 27, pp. 5459–5465, 2013.

[37] M. Azhar Uddin, H. Tsuda, S. Wu, and E. Sasaoka, “Catalytic decomposition of biomass tars with iron oxide catalysts,” *Fuel*, vol. 87, pp. 451–459, 2008.

[38] K. Polychronopoulou, a. Bakandritsos, V. Tzitzios, J. L. G. Fierro, and a. M. Efstathiou, “Absorption-enhanced reforming of phenol by steam over supported Fe catalysts,” *J. Catal.*, vol. 241, no. 1, pp. 132–148, 2006.

[39] M. Nakazawa and G. a. Somorjai, “Coadsorption of water and selected aromatic molecules to model the adhesion of epoxy resins on hydrated surfaces of zinc oxide and iron oxide,” *Appl. Surf. Sci.*, vol. 84, no. 3, pp. 309–323, 1995.

[40] K. Polychronopoulou, C. N. Costa, and a. M. Efstathiou, “The role of oxygen and hydroxyl support species on the mechanism of H 2 production in the steam reforming of phenol over metal oxide-supported-Rh and -Fe catalysts,” *Catal. Today*, vol. 112, no. 1–4, pp. 89–93, 2006.

[41] F. Lind, M. Seemann, and H. Thunman, “Continuous catalytic tar reforming of biomass derived raw gas with simultaneous catalyst regeneration,” *Ind. Eng. Chem. Res.*, vol. 50, no. 20, pp. 11553–11562, 2011.

[42] M. K. Eberhardt, “Reaction of Benzene Radical Cation with Water. Evidence for the Reversibility of OH Radical Addition to Benzene,” vol. 163, no. 1977, pp. 3876–3878, 1981.

[43] V. Hacker, R. Fankhauser, G. Faleschini, H. Fuchs, K. Friedrich, M. Muhr, and K. Kordesch, “Hydrogen production by steam-iron process,” *J. Power Sources*, vol. 86, no. 1, pp. 531–535, 2000.

[44] J. Francois, L. Abdelouahed, G. Mauviel, F. Patisson, O. Mirgaux, C. Rogaume, Y. Rogaume, M. Feidt, and a. Dufour, “Detailed process modeling of a wood gasification combined heat and power plant,” *Biomass and Bioenergy*, vol. 51, pp. 68–82, 2013.

[45] M. Barrio, B. Gøbel, H. Risnes, U. Henriksen, J. E. Hustad, N. K. Allé, and D.-K. Lyngby, “Steam gasification of wood char and the effect of hydrogen inhibition on the chemical kinetics .”

[46] A. Jess, “Mechanisms and kinetics of thermal reactions of aromatic hydrocarbons from pyrolysis of solid fuels,” *Fuel*, vol. 75, no. 12, pp. 1441–1448, 1996.

[47] F. Bustamante, R. M. Enick, a. V. Cugini, R. P. Killmeyer, B. H. Howard, K. S. Rothenberger, M. V. Ciocco, B. D. Morreale, S. Chattopadhyay, and S. Shi, “High-temperature kinetics of the homogeneous reverse water-gas shift reaction,” *AIChE J.*, vol. 50, no. 5, pp. 1028–1041, May 2004.

[48] F. Bustamante, R. M. Enick, R. P. Killmeyer, B. H. Howard, K. S. Rothenberger, a. V. Cugini, B. D. Morreale, and M. V. Ciocco, “Uncatalyzed and wall-catalyzed forward water-gas shift reaction kinetics,” *AIChE J.*, vol. 51, no. 5, pp. 1440–1454, May 2005.

[49] V. Spallina, P. Chiesa, E. Martelli, F. Gallucci, M. C. Romano, G. Lozza, and M. van Sint Annaland, “Reactor design and operation strategies for a large-scale packed-bed CLC power plant with coal syngas,” *Int. J. Greenh. Gas Control*, vol. 36, pp. 34–50, 2015.

[50] T. Pröll, K. Mayer, J. Bolhàr-Nordenkampf, P. Kolbitsch, T. Mattisson, A. Lyngfelt, and H. Hofbauer, “Natural minerals as oxygen carriers for chemical looping combustion in a dual circulating fluidized bed system,” *Energy Procedia*, vol. 1, no. 1, pp. 27–34, Feb. 2009.

[51] A.W. Coats and J. P. Redfern, “Thermogravimetric Analysis,” *Analyst*, vol. 88, no. 906, 1963.

[52] D. L. Pavia, G. M. Lampman, G. S. Kritz, and R. G. Engel, *Introduction to Organic Laboratory Techniques*, 4th editio. 2006.

[53] O. D. Sparkman, *Mass spectrometry desk reference*. Pittsburgh: Global View Pub., 2000.

[54] J. Goldstein, *Scanning electron microscopy and x-ray microanalysis*. Kluwer Adacemic/Plenum Pulbishers, 2003.

11. Appendix

11.1. Analysis techniques

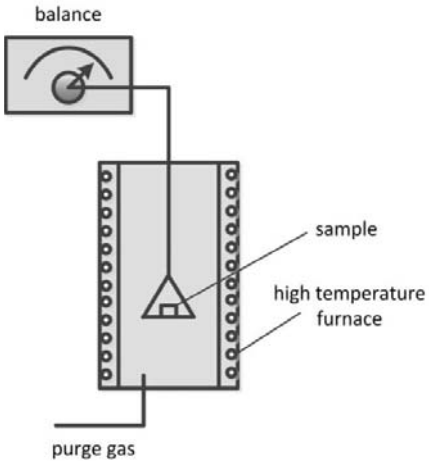

Fig. 53. Schematic overview of the thermogravimetric analysis apparatus.

11.1.1. Thermogravimetric analysis (TGA)

Thermogravimetric analysis (TGA) is a method in which the change in materials is analyzed after reaction with gases. The materials are characterized by measuring changes in physical and chemical properties either as a function of increasing temperature, with a constant heating rate, or as a function of time, with a constant temperature of mass loss. [51] The changes in physical and chemical properties involve the changes in weight, gas volume or pressure, solid volume, electrical resistance and ultraviolet, visible or infrared transmission of reflectance. For TGA experiments, the weight of the sample is monitored while the exiting gas of the TGA is analyzed with gas chromatography (GC) to find out what compounds are formed in during the reactions catalyzed by the oxygen carrier.

11.1.2. Gas chromatography (GC)

Gas chromatography (GC) is an analytic technique used for the identification of compounds in a mixture. An inert gas, such as helium or an unreactive gas such as nitrogen is used as the mobile phase of the gas chromatography. The stationary phase is a microscopic layer of liquid or polymer on a solid support, inside the column. The compounds that are analyzed, are gasified and interact with the walls of the column. Difference in interaction causes the compounds to elute at different times. Pure compounds are used for comparison in elution times [52].

11.1.3. Gas chromatography – mass spectrometry (GC-MS)

In gas chromatography – mass spectrometry (GC-MS), the features of GC are combined with mass spectrometry to indentify unknown substances in a sample. The compounds are separated with gas chromatography and then the molecules are identified by measuring the mass-to-charge ratio and abundance of gas-phase ions. Based on the mass spectrum, the possible molecules are identified and ordered by probability [53].

11.1.4. Scanning electron microscope (SEM)

A scanning electron microscope (SEM) produces images by scanning a surface with a focused beam of high-energy electrons. The electron interaction generates various signals that can be detected. These signals provide information about the external morphology, chemical composition, crystalline structure and orientation of the sample. Area's ranging from 2 cm to 5 µm in width can be imaged in a scanning electron microscope. It can achieve magnifications ranging from 20X to 30 000X and special resolutions of 50 to 100 nm [54].

11.1.5. Energy-dispersive X-ray spectroscopy (EDX)

Energy-dispersive X-ray spectroscopy (EDX) is an analytical technique used for elemental analysis of samples. EDX analyses the atomic structure of an element by its interaction with a source of excitation. It relies on the fundamental principle that all elements have a unique set of peaks in the X-ray emission spectrum. When combined with SEM, the X-ray spectrum is generated from the entire scan area of the SEM. The amount of X-ray counts processed by the detector are put on the Y-axis while the X-axis shows the energy level of those counts. The energy levels are associated with elements which makes identification possible [54].

11.2. Wet particle size distribution

A similar particle size of the catalytic samples is necessary to ensure that comparison of the overall kinetic data is fair. This is tested by size distribution analysis with laser diffraction.

11.2.1. Experimental set-up

The particle size distribution is analyzed using laser diffraction of a wet dispersion. The Wet Dispersion Unit ANALYSETTE 22 NanoTec plus of Fritsch is used. To degrade the strongly bound agglomerates, ultrasonic is utilized.

11.2.2. Results

The average particle size of olivine is 526 µm and the average particle size of ilmenite is 342 µm. These sizes are similar enough for comparison in a packed bed reactor. The peak in the olivine particle size is slightly wider. The graphs of the size distribution curves are shown below.

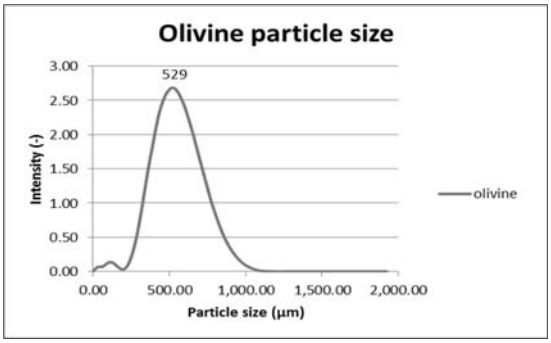

Fig. 54. Olivine particle size distribution.

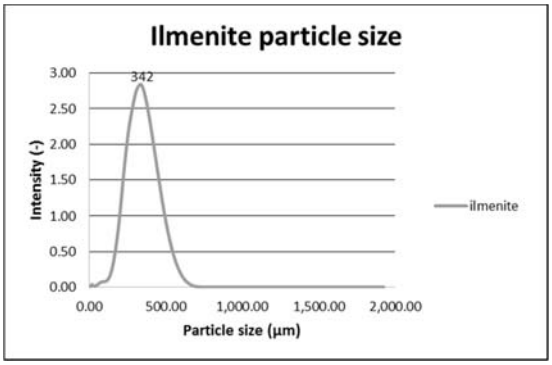

Fig. 55. Ilmenite particle size distribution.

11.3. Calibration curves of the mass flow controllers of the kinetics set-up

The mass flow controllers of the kinetics set-up are calibrated to ensure that the amount of gas put in at the controls represents the actual amount of gas flowing through the set-up.

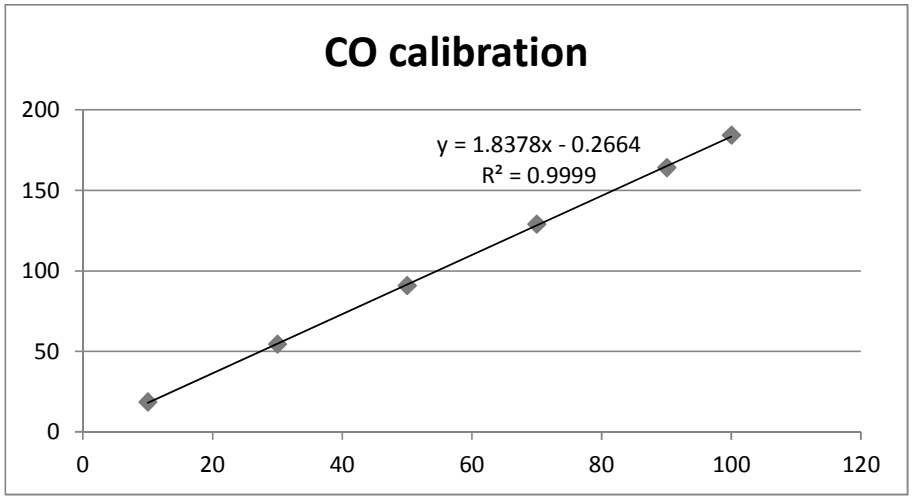

Fig. 56. CO calibration graph.

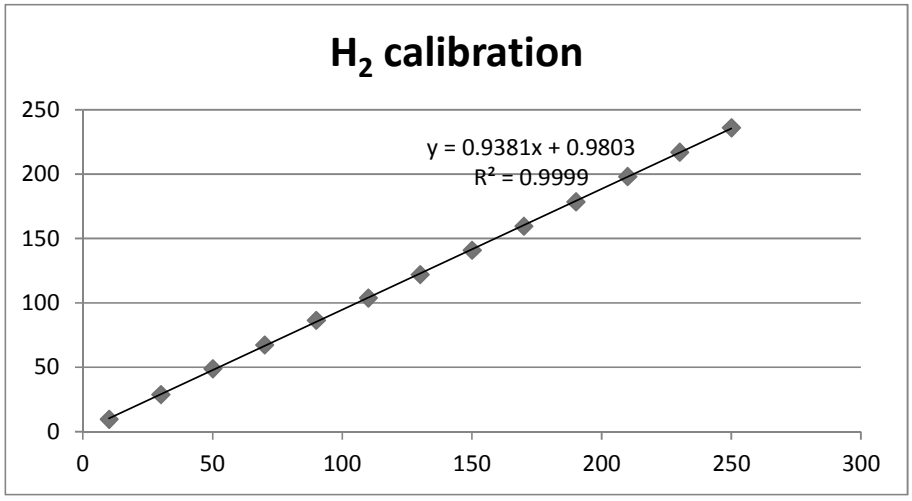

Fig. 57. H_2 calibration graph.

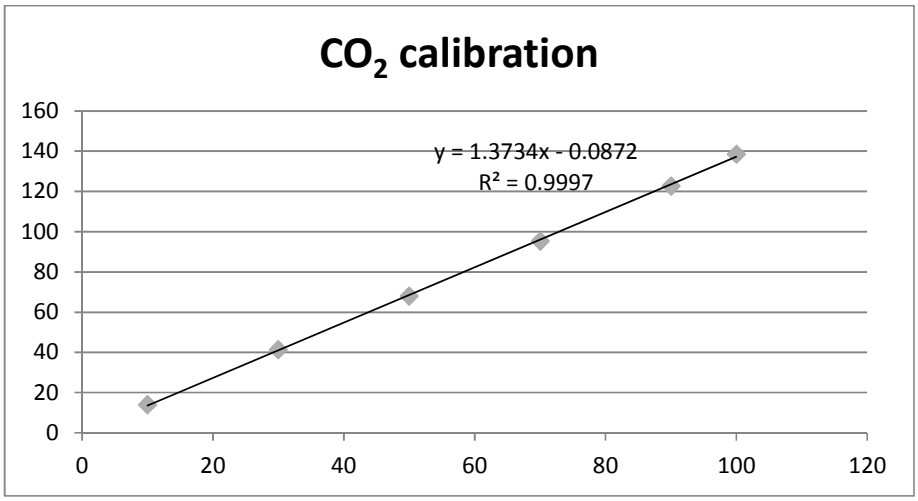

Fig. 58. CO_2 calibration graph.

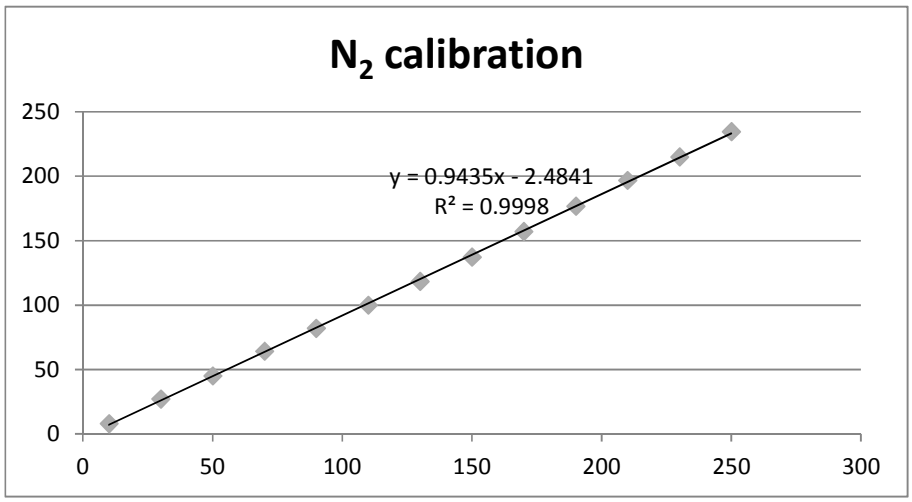

Fig. 59. N_2 calibration graph.

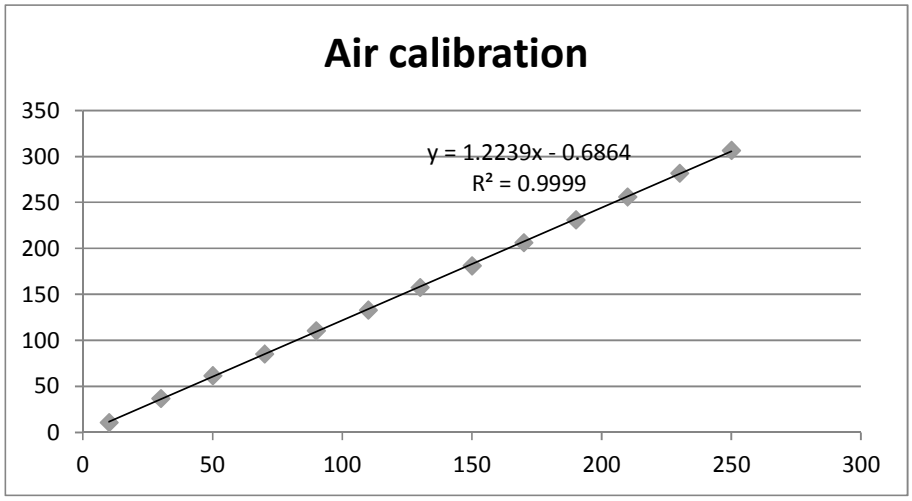

Fig. 60. Air calibration graph.

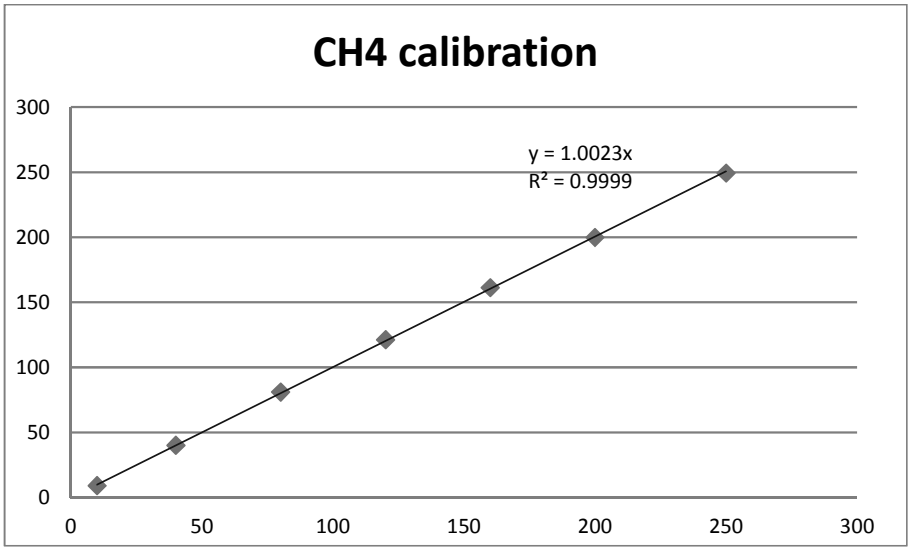

Fig. 61. Methane calibration graph.

11.4. Preliminary toluene steam reforming experiment with olivine

In the preliminary experiments, a temperature of 900 °C was used with olivine as an oxygen carrier. After these reactions, the reactor turned completely black. One set of results of these preliminary experiments is shown here. A picture of the blackened reactor is shown in figure 62. The experiment shown was done with 0.15 l/min of N_2, 0.5 g/min of H_2O and 0.35 g/min of C_7H_8. This corresponds to a steam to toluene ratio of 7 : 1. As can be seen in figure X, the amount of product gas at the outlet was very low and it shows the limitations of the analyzer. With a steam to toluene ratio of 7 : 1, water was close to limiting, which probably led to more carbon deposition. At this temperature, thermal cracking of toluene was detected in the blank experiments with toluene and water, which can add to the carbon deposition and the blackening of the reactor.

Fig. 62. Blackened reaction after toluene steam reforming reaction at 900 °C.

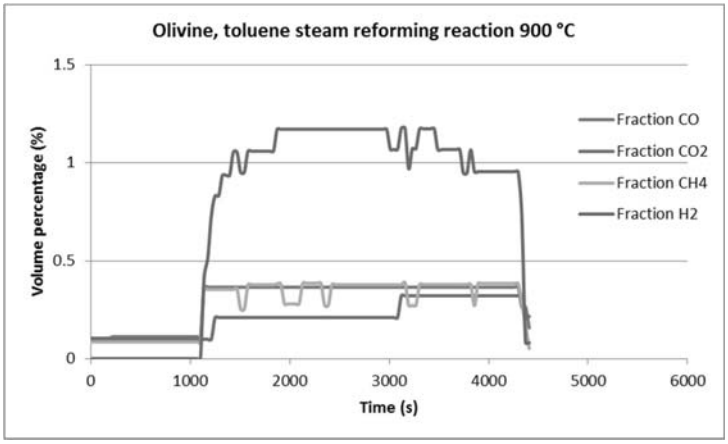

Fig. 63. Preliminary toluene steam reforming experiment with olivine at 900 °C.

11.5. GC calculations and spectra

To determine the toluene content of condensed samples from the kinetics set-up, the calculation on the following pages are used. The GC spectra of the different samples are included.

11.5.1. Toluene calibration line

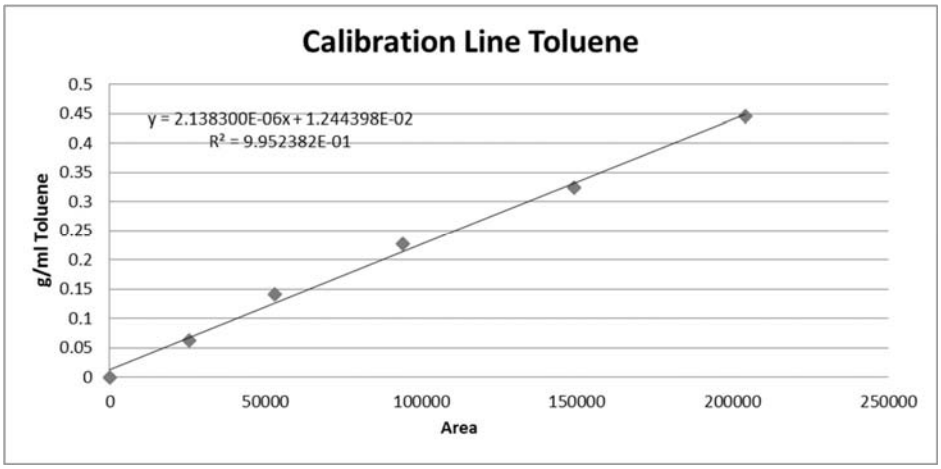

Fig. 64. Toluene calibration line.

Table 35. Toluene calibration calculations.

	Mw (g/mol)	densitiy (g/ml)		Flasks (mL)	0.5	
Heptane	100.21	0.684				
Toluene	92.14	0.866				
#	**Xtol**	**Th Heptane(g)**	**Th. Toluene(g)**	**Exp Heptane(g)**	**Exp Tol (g)**	**g/ml tol**
1	1	0.0000	0.4330	0	0.4573	0.4448
2	0.8	0.0887	0.3261	0.0811	0.3202	0.3240
3	0.6	0.1667	0.2299	0.1683	0.2291	0.2267
4	0.4	0.2346	0.1438	0.2353	0.1422	0.1410
5	0.2	0.2929	0.0673	0.2946	0.0621	0.0620
6	0	0.3420	0.0000	0.3429	0	0.0000

11.5.2. Olivine samples

The T stands for top phase and the B for bottom phase. Experiment 1 corresponds to the experiment with a steam to toluene ratio of 25 : 1. Experiment 2 has a steam to toluene ratio of 16 : 1.

Table 36. Olivine calculations for toluene content.

Measured cilinder volumes	Phase volume (mL)		
1T	2	2.468983435	Total toluene in experiment 1 (g)
1B	35		
2T	6	5.376997439	Total toluene in experiment 2 (g)
2B	22		

	Vial (g)	Vial +Sample (g)	V+S +Dilution (g)	Volume sample + dilution (mL)	Mass Sample (g)
1T	2.748	3.1856	3.5794	1	0.4376
1B	2.7212	3.2194	3.6118	1	0.4982
2T	2.7693	3.2036	3.5939	1	0.4343
2B	2.7623	3.2599	3.6551	1	0.4976

	A1	A2	A3	Average	stdev	rsd%
1T	175416.1	164529.4	168460.4	169468.6333	5512.935703	3.253071435
1B	672.7	639.8	664.3	658.9333333	17.09395605	2.594185964
2T	178040.7	180062.9	187435.3	181846.3	4944.695538	2.719162027
2B	154.7	145.9	146.8	149.1333333	4.841831609	3.246646139

	Toluene (g/mL) diluted sample	Toluene in sample (g)	Toluene (g/mL)	Toluene (mass fraction)
1T	0.374818759	0.374818759	0.749637517	0.856532812
1B	0.013852977	0.013852977	0.027705954	0.027806056
2T	0.401285923	0.401285923	0.802571847	0.923983245
2B	0.012762872	0.012762872	0.025525744	0.025648858

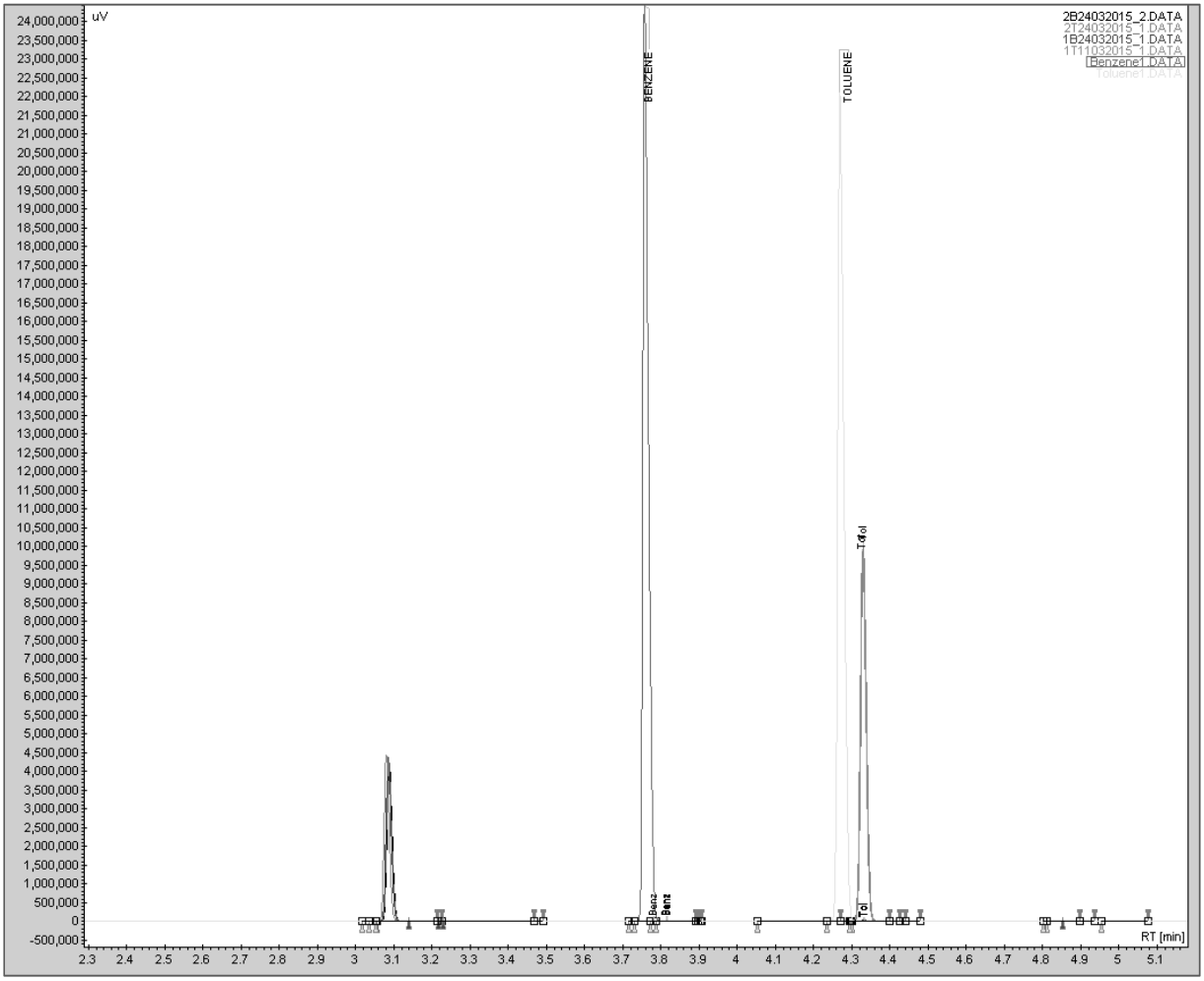

Fig. 65. GC spectrum of olivine sample 1 and 2, top and bottom phase.

The top and bottom phase for both toluene experiments with olivine are shown. In this spectrum, there is a reference peak for toluene and benzene. The peak to the left of that is an ethanol peak, used for quantification of the amount of toluene. Heptane is used for quantification as well, but is not shown in the spectrum.

11.5.3. Ilmenite samples

Only one sample has been quantified by GC. This is the sample with the 25 : 1 steam to toluene ratio.

	Vial (g)	Vial +Sample (g)	V+S +Dilution (g	Volume sample +	Mass Sample (g)
1T	2.7309	3.1671	3.561	1	0.4362
1B	2.7668	3.2659	3.6604	1	0.4991

	A1	A2	A3	Average	stdev	rsd%
1T	178707.9	188647.6	178927.1	182094.2	5676.469046	3.117325563
1B	158.8	175.8	153	162.5333333	11.84961321	7.290574168

	Toluene (g/mL) diluted sample	Toluene in sample (g)	Toluene (g/mL)	Toluene (mass fraction)
1T	0.401816008	0.401816008	0.803632016	0.921173792
1B	0.012791525	0.012791525	0.02558305	0.025629183

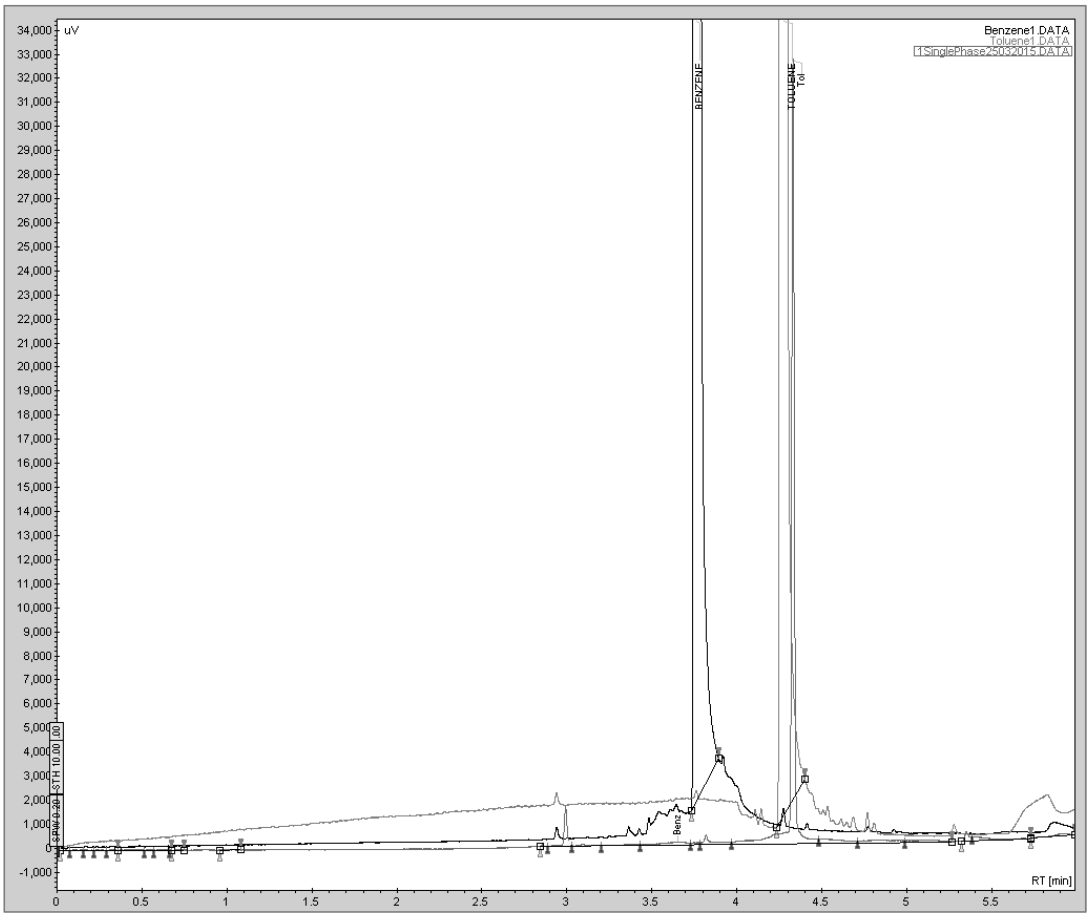

Fig. 66. GC spectrum of steam toluene reforming with ilmenite (25 : 1).

In figure 65, the GC spectrum of the first ilmenite experiment is shown. Many smaller peaks can be seen which indicates some impurities in the sample.

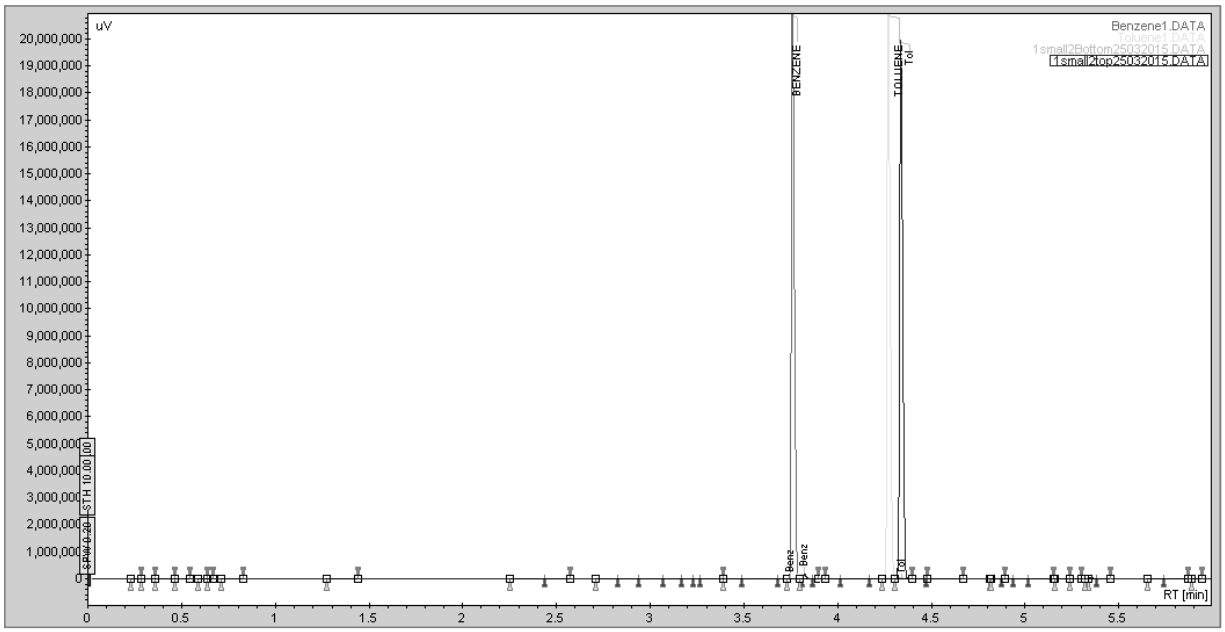

Fig. 67. GC spectrum of steam toluene reforming with ilmenite (16 : 1).

In figure 66, the GC spectrum of the second ilmenite experiment is shown. This sample is quite pure, as not many other small peaks appear.

11.6. GC-MS spectrum

The second ilmenite sample is investigated with GC-MS. The peaks that show in the GC-MS have a very low count. This indicates that impurities are very small, only traces of other components besides toluene are detected.

Ilmenite toluene steam reforming (16 : 1)

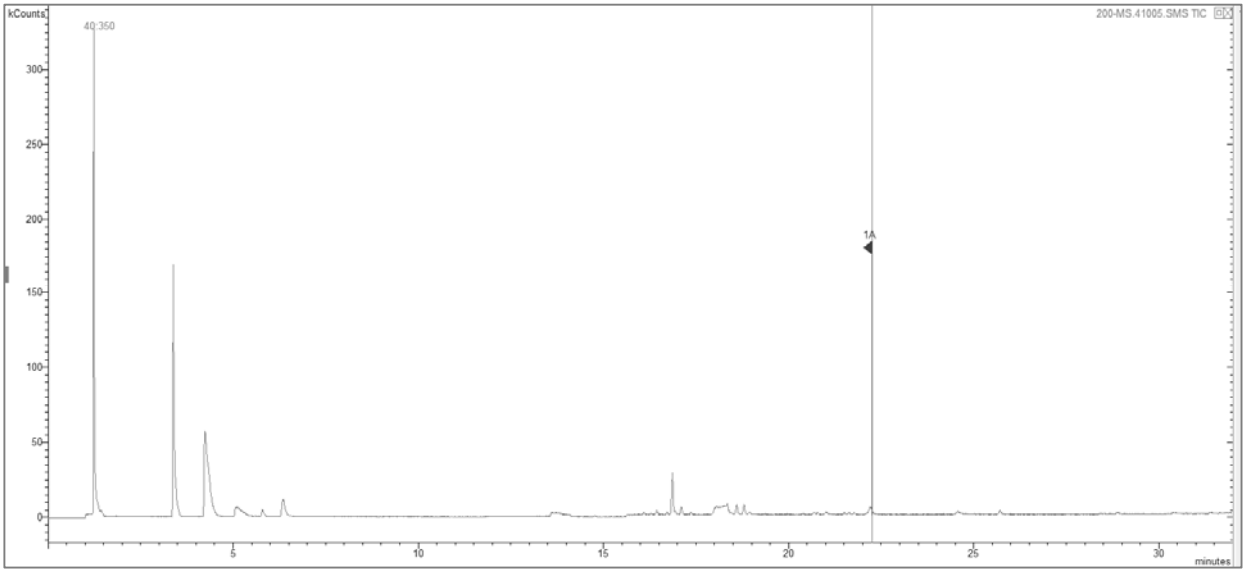

Fig. 68. GC-MS spectrum of toluene steam reforming on ilmenite (16 : 1).

11.7. EDX spectrum

As an example, the EDX spectrum and calculations of activated olivine are shown. The peaks are integrated to determine the surface content of a certain atom.

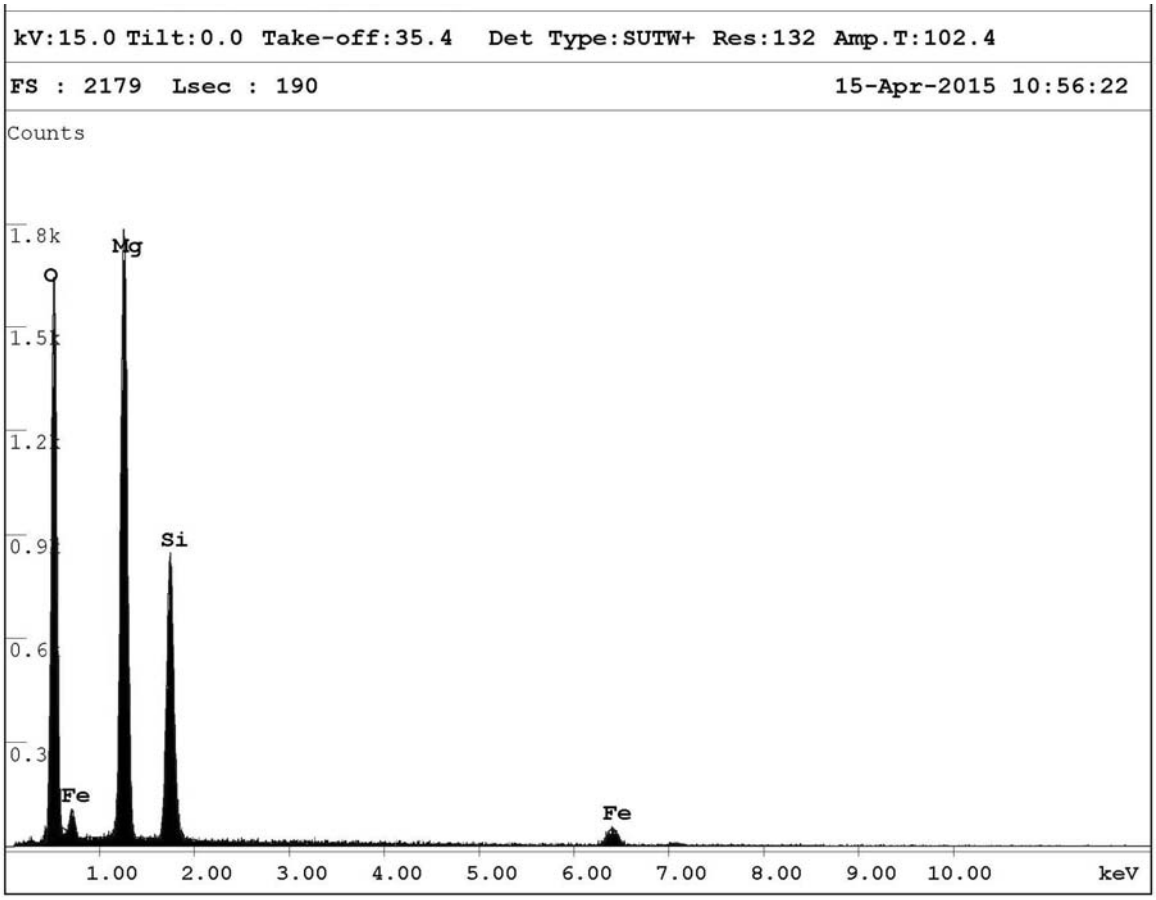

EDAX PhiRhoZ Quantification (Standardless)
Element Normalized
SEC Table : Default

Element	Wt %	At %
O K	40.34	53.77
MgK	33.12	29.05
SiK	18.65	14.16
FeK	7.90	3.02
Total	100.00	100.00

Element	Net Inte.	Bkgd Inte.	Inte. Error	P/B
O K	51.95	0.60	1.02	86.97
MgK	64.82	1.30	0.92	49.68
SiK	31.36	1.13	1.34	27.84
FeK	3.14	0.24	4.38	13.33

Fig. 69. EDX spectrum of activated olivine.

11.8. Comparison between Ni-olivine kinetics and experimental data for olivine

A comparison between Ni-olivine kinetics [23] and the experimental results for olivine was done in Aspen Plus. The used flowsheet can be seen in figure 69. The kinetic data of olivine doped with nickel were applied to a plug flow reactor of the same size as the experimental set-up. The experimental data were put into a yield reactor. The results are shown in table 35. The water-gas shift reaction was implemented as well. It is clear that the kinetic reaction for Ni-olivine was more active. It reached a toluene conversion of about 30 % while the experiments only reached 1 % conversion. With the flowsheet, it was estimated that the k value of the olivine from experiments was around 10^3 times smaller than the k value of olivine with nickel. No information about the activation energy could be estimated. A full kinetics study is necessary to determine the activation energy.

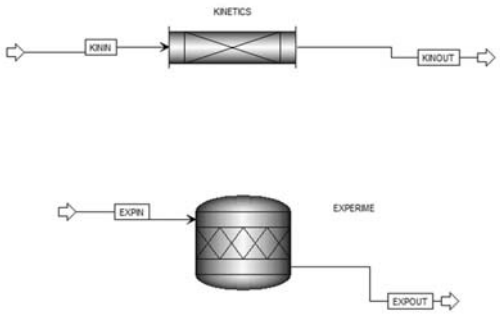

Fig. 70. Aspen Plus flowsheet for comparison of kinetics for toluene steam reforming with Ni-olivine and in olivine experiments.

Table 37. Results of the comparison of the kinetic data of toluene steam reforming with Ni-olivine to the data from experiments.

Flow	Unit	KININ	KINOUT	EXPIN	EXPOUT
H_2	kmol/hr	0	1.31027E-05	0	6.60947E-06
CO	kmol/hr	0	8.07564E-06	0	1.59539E-06
CO_2	kmol/hr	0	1.60398E-07	0	1.59539E-06
C_7H_6	kmol/hr	6.51179E-05	6.39414E-05	6.51179E-05	6.46621E-05
H_2O	kmol/hr	0.00166525	0.00165686	0.00166525	0.00166047